New fit to the reaction $\gamma p \to K^+\Lambda$

Alejandro de la Puente, Oren V. Maxwell, and Brian A. Raue
Department of Physics, Florida International University, University Park, Miami, Florida 33199, USA
(Received 29 September 2009; published 23 December 2009)

The reaction $\gamma p \to K^+\Lambda$ has been investigated over the center-of-momentum energy, W, range from threshold up to 2.2 GeV in a tree-level effective Lagrangian model that incorporates most of the well-established baryon resonances with spins equal to or below $\frac{5}{2}$. Four less well-established nucleon resonances of higher mass are also included. The fitted parameters consist, for each resonance included, of the products of the coupling strengths at the electromagnetic and strong interaction vertices and, for the less-established nucleon resonances, of the total decay width. For the well-established nucleon resonances, the energy and momentum dependence of the widths are treated within a dynamical model that is normalized to give the empirical decay branching ratios on the resonance mass shells. For the less-established resonances, the total decay width is treated as a single parameter independent of the reaction kinematics. The model is used to fit recent data for the unpolarized differential cross section (CLAS), the induced hyperon polarization asymmetry, P (CLAS, GRAAL, SAPHIR), the beam spin asymmetry, Σ (LEPS and GRAAL), and the double-polarization observables C_x and C_z (CLAS). The model results were also compared with LEPS data for the unpolarized differential cross section, but those data were not included in the fit. Two different fits were obtained: one that incorporates SU(3)-symmetry constraints on the Born contributions to the reaction amplitude and one in which these constraints are relaxed. Explicit numerical results are given only for the first fit because the two fits gave nearly identical results for the observables and the χ^2 per degree of freedom obtained with the second fit was only marginally better than that of the first fit ($<1\%$ better). Results are presented for the fitted observables at several different energies and center-of-momentum (CM) frame kaon angles.

DOI: 10.1103/PhysRevC.80.065205 PACS number(s): 25.10.+s, 25.20.Lj, 13.60.−r

I. INTRODUCTION

Interest in the electromagnetic production of strangeness from few-nucleon targets, such as the proton and the deuteron, dates back to the 1960s [1–3], but it is comparatively recently that high-quality data, suitable for quantitatively testing theoretical models, has become available [4–13]. The strangeness degree of freedom imparts to these reactions the potential to provide fundamental information concerning both the strong and electromagnetic interactions beyond that obtainable from reactions involving just the nonstrange baryons. Within an effective Lagrangian model, one could use these reactions to search for baryon resonances that decay to strange particles and possibly test SU(3)-symmetry relations among the couplings of resonances within the same SU(3) multiplets. By comparing photoproduction and electroproduction results, one might be able to extract information concerning the electromagnetic form factors of baryon resonances. Finally, with the aid of a quantitative model for electromagnetic strangeness production from the proton, one could, within the impulse approximation, use results for strangeness production from the deuteron and other light nuclei to study final state interactions involving the Λ and Σ baryons.

Much of the theoretical work over the past 20 years or so has been based on effective Lagrangian models [14–28]. Recently, there have been several coupled-channel analyses [29–32] that have revealed the need for resonances that had not been previously included in many of the effective Lagrangian models. Until recently, the fits and models were largely based on older data and often combined photoproduction data and electroproduction data to generate the fits. More recent fits have made use of various combinations of recent data from the SAPHIR [4], CLAS [8,10,11], LEPS [5], and GRAAL [9] Collaborations.

In Ref. [27], it was suggested that the photoproduction data and the electroproduction data should *not* be fit together; rather one should first generate a model for the basic reaction using photoproduction data alone and then use that model, in conjunction with electroproduction data, to obtain information concerning the electromagnetic form factors of the various resonances in the model. This consideration, along with the abundance of new data, particularly, polarization data, has motivated us to develop a new model for the reaction $\gamma p \to K^+\Lambda$ over the energy range from threshold up to a center-of-momentum (CM) energy of 2.2 GeV. Although the CLAS data extend up to 2.6 GeV, the lack of s-channel resonances in our model with masses above 2.2 GeV precludes a reliable treatment of the higher energy data. As discussed in Sec. IV, the fits involve a subtle interference between s-channel contributions to the reaction on the one hand and u- and t-channel contributions on the other hand, which, to be effective, requires that the s-channel resonances included in a particular fit have masses spanning the whole energy range of that fit.

The model is similar to that described in Refs. [25–27] but has been expanded to include spin $\frac{5}{2}$ baryon resonances in both the s and u channels, in addition to the spin $\frac{1}{2}$ and spin $\frac{3}{2}$ resonances included in the earlier work. This model also includes several higher energy, less well-established resonances in the s channel that were not included in the earlier work. Finally, the fits described here are much more

elaborate than those described in Refs. [25–27] in that both single- and double-polarization data are included in our fits. The reaction model is described in some detail in Sec. II.

Two separate fits were generated. The first fit has SU(3)-symmetry constraints imposed on the Born terms in all three channels. These constraints, along with inputted empirical values for the baryon magnetic moments, require particular relationships between the various Born terms and also, in conjunction with other considerations, provide a range of values for the ΛKN coupling. This is discussed more fully in Sec. III. In the second fit, the ΛKN coupling was allowed to move outside the SU(3)-symmetry range and assume whatever value yielded the best fit to the data. The second fit obtained is nearly identical to the first fit and yielded a χ^2 per degree of freedom that differs from that of the first fit by less than 1%. For these reasons, only results derived from the first fit are presented here.

We have used all recently published results for the spin observables, P [4,8,9], Σ [5,9], C_x, and C_z [11] in our fits. Because there appear to be some inconsistencies in cross-section data obtained by different groups [33], we have used only the most recently published cross-section data from the CLAS Collaboration [10] in the fits but have compared the fit results for the cross section with recent LEPS data [5]. Further details concerning the fitting procedure are contained in Sec. III.

The resulting fit, along with several figures illustrating the quality of the fits, are presented and discussed in Sec. IV. Section IV also contains some concluding remarks and a brief discussion of future work.

II. THE REACTION MODEL

The reaction model incorporates contributions in the s, u, and t channels. These are illustrated in Fig. 1. The s-channel contributions include the Born term with an intermediate proton and contributions in which an intermediate nucleon resonance is excited. Similarly, the u-channel Born contributions with the excitation of an intermediate Λ or Σ baryon are supplemented by contributions involving the excitation of an intermediate hyperon resonance. In the t channel, contributions from both $K^\star(892)$ and $K1(1270)$ exchange are included, as well as the Born contribution involving ground-state kaon exchange.

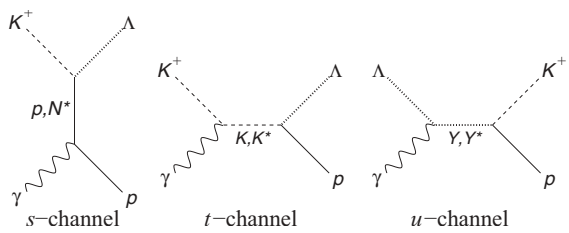

FIG. 1. Contributions to the amplitude for the reaction $\gamma p \to K^+\Lambda$.

In the various channels, the reaction amplitudes have the general forms

$$\hat{T}_s = \sum_{N^\star} \mathcal{V}_K^\dagger(p_K) D(p_s) \mathcal{V}_\gamma(p_\gamma), \tag{1}$$

$$\hat{T}_u = \sum_{Y^\star} \mathcal{V}_\gamma^\dagger(p_\gamma) D(p_u) \mathcal{V}_K(p_K), \tag{2}$$

and

$$\hat{T}_t = \sum_{K^\star} \mathcal{V}_{\gamma K}^\dagger(p_\gamma, p_t) D_t(p_t) \mathcal{V}_{p\Lambda}(p_t), \tag{3}$$

where $p_s = p_\Lambda + p_K$, $p_u = p_\Lambda - p_\gamma$, and $p_t = p_\gamma - p_K$ are the intermediate four-momenta in the various channels, the $\mathcal{V}$'s are the electromagnetic and strong interaction vertices, and the D's are the associated intermediate baryon and meson propagators. In all channels, the forms of both the electromagnetic vertices and the strong interaction vertices depend on the spin and the parity of the intermediate hadron that is excited.

In the t channel, the two vertices are given by

$$\mathcal{V}_{\gamma K} = -e\epsilon \cdot (p_K - p_t) \tag{4}$$

and

$$\mathcal{V}_{p\Lambda} = g_{\Lambda K p}\gamma_5 \tag{5}$$

for an intermediate ground-state kaon (the t-channel Born term), by

$$\mathcal{V}^\mu_{\gamma K} = \frac{g_{\gamma K K^\star}}{m_{\rm sc}} \epsilon^{\mu\nu\rho\lambda} \epsilon_\nu p_{\gamma\rho} p_{t\lambda} \tag{6}$$

and

$$\mathcal{V}^\mu_{p\Lambda} = \left(g^V_{\Lambda K^\star p} + \frac{g^T_{\Lambda K^\star p}}{m_p + m_\Lambda} \gamma \cdot p_t \right) \gamma^\mu \tag{7}$$

for an intermediate $K^\star(892)$ resonance, and by

$$\mathcal{V}^\mu_{\gamma K} = \frac{g_{\gamma K K1}}{m_{\rm sc}} \left(\epsilon \cdot p_t p^\mu_\gamma - p_\gamma \cdot p_t \epsilon^\mu \right) \tag{8}$$

and

$$\mathcal{V}^\mu_{p\Lambda} = \left(g^V_{\Lambda K1 p} + \frac{g^T_{\Lambda K1 p}}{m_p + m_\Lambda} \gamma \cdot p_t \right) \gamma^\mu \gamma_5 \tag{9}$$

for an intermediate $K1(1270)$ resonance. Here, ϵ is the photon polarization four-vector and $m_{\rm sc}$ is a scaling mass, set equal to 1000 MeV, that is introduced to make the electromagnetic coupling strengths dimensionless. The corresponding kaon resonance propagators both have the same form:

$$D_t = \frac{-g_{\mu\nu} + \frac{p_{t\mu} p_{t\nu}}{m^2_{K^\star}}}{p_t^2 - m^2_{K^\star}}, \tag{10}$$

where the label $K^\star$ now refers to either of the two resonances. We note that the propagator employed here, in contrast with that used in Refs. [25–27], does not contain a width because the intermediate energies in the t channel lie well below the thresholds of any possible decay channels.

In the s- and u-channel Born contributions and in those contributions arising from the excitation of intermediate spin $\frac{1}{2}$ resonances, we employ standard expressions for the

electromagnetic vertices and use the pseudoscalar form for the strong interaction vertices. For positive-parity intermediate baryons, this gives

$$\mathcal{V}_{K\,\frac{1}{2}^+}(p_K) = g\gamma_5 \tag{11}$$

and

$$\mathcal{V}_{\gamma\,\frac{1}{2}^+}(p_\gamma) = g_\gamma \epsilon_\mu i\sigma^{\mu\nu}(p_\gamma)_\nu \tag{12}$$

with

$$g_\gamma = \frac{e\kappa}{2m_B}, \tag{13}$$

where κ is defined by its relation to the transition magnetic moment,

$$\mu_T = \frac{e\kappa}{m_B + m_I}, \tag{14}$$

m_B is the mass of the incoming or outgoing baryon (m_p or m_Λ), and m_I is the mass of the intermediate baryon. The corresponding expressions for negative-parity intermediate baryons just have the γ_5 factor transposed from the strong interaction vertex to the electromagnetic vertex. For intermediate protons, there is an additional term,

$$\mathcal{V}_{\rm charge}(p_\gamma) = e\gamma^\mu \epsilon_\mu, \tag{15}$$

arising from the proton's charge. For the spin $\frac{1}{2}$ propagator, we employ, in agreement with other authors, a relativistic Breit-Wigner form,

$$D^{\frac{1}{2}}(p) = \frac{\gamma\cdot p + m_I}{p^2 - m_I^2 + i m_I \Gamma_I}, \tag{16}$$

where the width Γ_I is nonzero only in the s-channel resonance contributions.

In the s- and u-channel contributions from intermediate spin $\frac{3}{2}$ baryons, several different forms have been employed for the vertices and the propagator. The authors of Ref. [14] introduced a form for the spin $\frac{3}{2}$ propagator in the s channel in which the intermediate baryon mass appearing in the numerator and projection operator of the Rarita-Schwinger propagator was replaced by $\sqrt{s}$. This was motivated by the desire to ensure gauge invariance off-shell. However, use of the same prescription in the u channel leads to unphysical singularities. Moreover, as pointed out in Ref. [34], the propagator employed in Ref. [14] does not satisfy the differential equation that defines the propagator as a Green's function. For these reasons, we employ the standard Rarita-Schwinger form for the spin $\frac{3}{2}$ propagator and use forms for the corresponding vertices that are similar to those introduced in Ref. [21]. However, in contrast to the work of Ref. [21], we make no attempt to include off-shell terms in the vertices. The results reported in Ref. [21] suggest that these terms, as well as off-shell terms in the propagator, have a relatively modest effect on the calculated observables. The resulting vertices for positive-parity spin $\frac{3}{2}$ intermediate baryons take the forms

$$\mathcal{V}^\mu_{K\,\frac{3}{2}^+}(p_K) = -\frac{g}{m_\pi} p_K^\mu \tag{17}$$

and

$$\mathcal{V}^\mu_{\gamma\,\frac{3}{2}^+}(p_\gamma) = \left[\frac{g_1}{2m_B}\left(\epsilon^\mu \gamma\cdot p_\gamma - p_\gamma^\mu \gamma\cdot\epsilon\right) + \frac{g_2}{4m_B^2}\left(\epsilon\cdot p_B p_\gamma^\mu - p_\gamma\cdot p_B \epsilon^\mu\right)\right]\gamma_5, \tag{18}$$

where p_B is the four-momentum of the incoming or outgoing ground-state baryon. As for the spin $\frac{1}{2}$ contributions, the negative-parity vertices just have the γ_5 factor transposed from one vertex to the other vertex. Note in these expressions that the strong interaction coupling has been divided by the pion mass, rather than by the kaon mass as in Ref. [21]. This makes it easier to compare our coupling strengths with the corresponding pion couplings for the purpose of testing SU(3)-symmetry relations among the couplings. The Rarita-Schwinger propagator is obtained by multiplying the spin $\frac{1}{2}$ propagator given by Eq. (16) on the right by the spin $\frac{3}{2}$ projection operator

$$P^{\frac{3}{2}}_{\mu\nu} = g_{\mu\nu} - \frac{1}{3}\gamma_\mu\gamma_\nu + \frac{1}{3}\frac{p_\mu\gamma_\nu - p_\nu\gamma_\mu}{m_I} - \frac{2}{3}\frac{p_\mu p_\nu}{m_I^2}. \tag{19}$$

With the exception of Ref. [20], most of the earlier work on the photoproduction of strangeness does not include contributions from intermediate states with spin $\frac{5}{2}$, even though there are several well-established baryon resonances with this spin below 2 GeV. Reference [20] and some of the later work do include spin $\frac{5}{2}$ resonances in the s channel but not in the u channel. To our knowledge, this work is the first analysis to include resonances with spin greater than $\frac{3}{2}$ in *both* the s and u channels. For the spin $\frac{5}{2}$ vertices, we employ forms similar to those given in Ref. [20] but modified so as to be consistent with the forms adopted here for the spin $\frac{3}{2}$ vertices. Again, we do not include any off-shell terms in the spin $\frac{5}{2}$ vertices. For positive-parity intermediate resonances, the resulting vertices are given by

$$\mathcal{V}^{\mu\nu}_{K\,\frac{5}{2}^+}(p_K) = \frac{g}{m_\pi^2} p_K^\mu p_K^\nu \gamma_5 \tag{20}$$

and

$$\mathcal{V}^{\mu\nu}_{\gamma\,\frac{5}{2}^+}(p_\gamma) = \left[\frac{g_1}{2m_B}\left(\epsilon^\mu \gamma\cdot p_\gamma - p_\gamma^\mu \gamma\cdot\epsilon\right) + \frac{g_2}{4m_B^2}\left(\epsilon\cdot p_B p_\gamma^\mu - p_\gamma\cdot p_B \epsilon^\mu\right)\right]\frac{p_\gamma^\nu}{m_\pi}. \tag{21}$$

As for the other s- and u-channel vertices, the corresponding negative-parity vertices just have the γ_5 factor transposed from one vertex to the other vertex. The corresponding propagator is constructed by multiplying the spin $\frac{1}{2}$ propagator on the right by the spin $\frac{5}{2}$ projector operator,

$$P^{\frac{5}{2}}_{\mu\nu,\mu'\nu'} = R_{\mu\nu,\mu'\nu'} - \tfrac{1}{5}P_{\mu\nu}P_{\mu'\nu'} - \tfrac{1}{5}(P_{\mu\rho}\gamma^\rho\gamma^\sigma R_{\sigma\nu,\mu'\nu'} + P_{\nu\rho}\gamma^\rho\gamma^\sigma R_{\sigma\mu,\mu'\nu'}) \tag{22}$$

with

$$R_{\mu\nu,\mu'\nu'} = \tfrac{1}{2}(P_{\mu\mu'}P_{\nu\nu'} + P_{\mu\nu'}P_{\nu\mu'}), \tag{23}$$

where

$$P_{\mu\nu} = g_{\mu\nu} - p_\mu p_\nu / m_I^2. \tag{24}$$

A. *s*-channel resonance widths

The intermediate nucleon resonances excited in the s channel generally lie at energies above the thresholds for decay into various decay channels. Thus, the propagators employed for the s-channel resonances need to include widths, and these widths are generally required rather far off the resonance mass shells. Most previous studies have ignored the off-shell nature of the resonances and simply have used the on-shell values of the widths. In Ref. [25], a model was proposed to dynamically generate widths off-shell by making use of partial width data summarized in the particle data tables [35]. The full width is first decomposed into a number of different decay channels. In each such channel, the off-shell energy and momentum dependence of the partial width is then treated using an effective Lagrangian model with the required coupling strength adjusted to yield the empirical on-shell branching ratio for decay into that channel. Two types of decays are considered: two-body decays in which both decay products are stable under the strong interaction, and decays in which one of the decay products is itself unstable, so that ultimately more than two decay products result.

Decays of the first type all involve the decay of a nucleon resonance into a pseudoscalar meson and a spin $\frac{1}{2}$ ground-state baryon. In the resonance rest frame, the corresponding widths are given by the expressions

$$\Gamma\left(\frac{1}{2}^+ \to \frac{1}{2}^+ + 0^-\right) = \frac{f^2}{4\pi}\frac{p}{\sqrt{s}}\left[E_B - m_B\right], \tag{25}$$

$$\Gamma\left(\frac{1}{2}^- \to \frac{1}{2}^+ + 0^-\right) = \frac{f^2}{4\pi}\frac{p}{\sqrt{s}}\left[E_B + m_B\right], \tag{26}$$

$$\Gamma\left(\frac{3}{2}^+ \to \frac{1}{2}^+ + 0^-\right) = \frac{f^2}{12\pi}\frac{p^2}{m_\pi^2}\frac{p}{\sqrt{s}}\left[E_B + m_B\right], \tag{27}$$

$$\Gamma\left(\frac{3}{2}^- \to \frac{1}{2}^+ + 0^-\right) = \frac{f^2}{12\pi}\frac{p^2}{m_\pi^2}\frac{p}{\sqrt{s}}\left[E_B - m_B\right], \tag{28}$$

$$\Gamma\left(\frac{5}{2}^+ \to \frac{1}{2}^+ + 0^-\right) = \frac{f^2}{30\pi}\frac{p^4}{m_\pi^4}\frac{p^3}{\sqrt{s}(E_B + m_B)}, \tag{29}$$

and

$$\Gamma\left(\frac{5}{2}^- \to \frac{1}{2}^+ + 0^-\right) = \frac{f^2}{30\pi}\frac{p^4}{m_\pi^4}\frac{p(E_B + m_B)}{\sqrt{s}} \tag{30}$$

for the pseudoscalar meson decays, where p is the channel momentum and m_B and E_B are the mass and energy of the baryon decay product. To obtain the total contribution to the width from two-body channels at a particular energy, the partial widths are summed over all two-body decay channels open at that particular energy.

Any part of the full on-shell decay width not accounted for by the two-body decays discussed earlier is attributed to decays in which one of the decay products is itself unstable under the strong interaction. These latter decays are approximated either as decays into a ground-state baryon and a meson resonance or as decays into a ground-state meson and a baryon resonance. In practice, for the low-lying nucleon resonances, only decays into the $N\sigma$, $N\rho$, and $\Delta(1232)\pi$ channels are considered. The $N\sigma$ channel is treated as a decay into a nucleon and a scalar meson of zero width. The corresponding decay widths are the same as those for two-body pseudoscalar decays of resonances with the opposite parity.

The two remaining channels both involve a stable ground-state hadron and an unstable resonance that itself has a width. To treat such decays, we employ the method developed in Ref. [25], which involves an integration over the unstable decay product mass of the decay phase-space factor multiplied by a Breit-Wigner distribution function. In particular, for decay into either channel, the partial width is given by the general expression

$$\Gamma(s) = \frac{g^2}{4\pi}\int_{m_{\min}}^{m_{\max}} \mathcal{P}(s,x)\mathcal{S}(x)dx, \tag{31}$$

where g is the coupling strength, $\mathcal{P}$ is the decay phase-space factor, and the integration limits are defined by

$$\begin{aligned} m_{\min} &= \sqrt{s_{\text{thr}}} - m_{\text{stable}}, \\ m_{\max} &= \sqrt{s} - m_{\text{stable}}. \end{aligned} \tag{32}$$

In the last expressions, $\sqrt{s_{\text{thr}}}$ is the threshold value of the center-of-momentum energy for decay into that channel and m_{stable} is the stable decay product mass (either m_N or m_π). The Breit-Wigner distribution function has the form

$$\mathcal{S}(x) = \frac{A}{2\pi}\frac{\Gamma_{\text{pr}}}{(x - m_C)^2 + \frac{1}{4}\Gamma_{\text{pr}}^2}, \tag{33}$$

where Γ_{pr} is the unstable decay product width, m_C is the mass of the unstable decay product at the center of its mass distribution, and the parameter A is defined by the normalization requirement

$$\int_{m_{\min}}^{\infty} \mathcal{S}(x)dx = 1. \tag{34}$$

The vertices for decays of spin $\frac{1}{2}$ resonances into the $\Delta(1232)\pi$ channel are related to those for decays of spin $\frac{3}{2}$ resonances into the $N\pi$ channel by just the interchange of the initial and final baryon states. The vertices for decays of spin $\frac{3}{2}$ and spin $\frac{5}{2}$ resonances into the $\Delta(1232)\pi$ channel each involve two independent couplings, only one of which can be fixed by the on-shell partial width. To avoid this difficulty, we keep, in each case, only the coupling of lowest order in the channel momentum. With that proviso, the phase-space factors for decays into the $\Delta(1232)\pi$ channel are given by

$$\mathcal{P}\left(\frac{1}{2}^+ \to \frac{3}{2}^+ + 0^-\right) = \frac{2}{3}\frac{p^2}{m_\pi^2}\frac{s}{x^2}\frac{p}{\sqrt{s}}(E + x), \tag{35}$$

$$\mathcal{P}\left(\frac{1}{2}^- \to \frac{3}{2}^+ + 0^-\right) = \frac{2}{3}\frac{p^2}{m_\pi^2}\frac{s}{x^2}\frac{p}{\sqrt{s}}(E - x), \tag{36}$$

$$\mathcal{P}\left(\frac{3}{2}^+ \to \frac{3}{2}^+ + 0^-\right) = \frac{5}{9}\frac{p}{\sqrt{s}}(E - x), \tag{37}$$

$$\mathcal{P}\left(\frac{3}{2}^- \to \frac{3}{2}^+ + 0^-\right) = \frac{p}{\sqrt{s}}(E+x), \tag{38}$$

$$\mathcal{P}\left(\frac{5}{2}^+ \to \frac{3}{2}^+ + 0^-\right) = \frac{1}{3}\frac{p^2}{m_\pi^2}\frac{p(E+x)}{\sqrt{s}}, \tag{39}$$

and

$$\mathcal{P}\left(\frac{5}{2}^- \to \frac{3}{2}^+ + 0^-\right) = \frac{7}{45}\frac{p^2}{m_\pi^2}\frac{p^3}{\sqrt{s}(E+x)}, \tag{40}$$

where x is the mass that is integrated over in the mass distribution, p is the channel momentum for that value of x, and $E = \sqrt{x^2+p^2}$.

Like the decays of spin $\frac{3}{2}$ and spin $\frac{5}{2}$ resonances into the $\Delta(1232)\pi$ channel, decays into the $N\rho$ channel generally involve vertices with two independent couplings. For the spin $\frac{1}{2}$ resonances decays, we adopt the same procedure as used in Ref. [25]. For the spin $\frac{3}{2}$ and spin $\frac{5}{2}$ resonance decays, we simply drop the couplings of higher order in the momenta and energies. This yields the phase-space factors

$$\mathcal{P}\left(\frac{1}{2}^+ \to \frac{1}{2}^+ + 1^-\right) = \frac{p^2}{x^2}\frac{p}{\sqrt{s}}\frac{(E_+-E)^2+2x^2}{E_+}, \tag{41}$$

$$\mathcal{P}\left(\frac{1}{2}^- \to \frac{1}{2}^+ + 1^-\right) = \frac{p^2}{x^2}\frac{p}{\sqrt{s}}\frac{(E_--E)^2+2x^2}{E_-}, \tag{42}$$

$$\mathcal{P}\left(\frac{3}{2}^+ \to \frac{1}{2}^+ + 1^-\right) = \frac{1}{24}\frac{p^2}{x^2}\frac{p}{\sqrt{s}}\frac{2(E^2+p^2)^2+x^2(E_+-E)^2+3x^2(E_++E)^2}{E_+m_B^2}, \tag{43}$$

$$\mathcal{P}\left(\frac{3}{2}^- \to \frac{1}{2}^+ + 1^-\right) = \frac{1}{24}\frac{p^2}{x^2}\frac{p}{\sqrt{s}}\frac{2(E^2+p^2)^2+x^2(E_--E)^2+3x^2(E_-+E)^2}{E_-m_B^2}, \tag{44}$$

$$\mathcal{P}\left(\frac{5}{2}^+ \to \frac{1}{2}^+ + 1^-\right) = \frac{1}{30}\frac{p^2}{m_\pi^2}\frac{p}{\sqrt{s}}\frac{E_+}{m_B^2}(A_+^2+2B_+^2+C_+^2), \tag{45}$$

and

$$\mathcal{P}\left(\frac{5}{2}^- \to \frac{1}{2}^+ + 1^-\right) = \frac{1}{30}\frac{p^2}{m_\pi^2}\frac{p}{\sqrt{s}}\frac{E_+}{m_B^2}(A_-^2+2B_-^2+C_-^2), \tag{46}$$

where

$$\begin{aligned} A_+ &= \sqrt{s}-m_B \\ B_+ &= \frac{p^2}{E_+}-\frac{A_+}{2} \\ C_+ &= \frac{EA_+}{x}+\frac{p^2(E_+-E)}{xE_+} \end{aligned} \tag{47}$$

and

$$\begin{aligned} A_- &= \frac{p}{E_+}(\sqrt{s}+m_B) \\ B_- &= p\left(1-\frac{\sqrt{s}+m_B}{2}\right) \\ C_- &= \frac{p}{x}\frac{E^2+p^2}{E_+} \end{aligned} \tag{48}$$

with $E_+ = E_B + m_B$ and $E_- = E_B - m_B$.

The dynamic width model described was employed for all of the three- and four-star status s-channel resonances used in the fits. For these well-established resonances, there are generally enough branching ratio data that reasonably good estimates for the partial widths on the resonance mass shells can be generated. For the higher energy, less well-established resonances, this is generally not the case. Hence, for these resonances, we employ energy-independent widths that are treated as parameters to be varied in the fits.

B. Evaluation of the matrix elements

The matrix elements for the reaction $\gamma p \to K^+\Lambda$ have the general structure

$$\begin{aligned} &\bar{u}_{M_\Lambda}(p_\Lambda)\hat{T}u_{M_p}(p_p) \\ &\quad = \bar{u}_{M_\Lambda}(p_\Lambda)[\hat{A}+\hat{B}\gamma_5+\hat{C}\gamma^0+\hat{D}\gamma^0\gamma_5]u_{M_p}(p_p), \end{aligned} \tag{49}$$

where p_p and M_p are the four-momentum and spin projection of the proton and p_Λ and M_Λ are the four-momentum and spin projection of the Λ. The operators $\hat{A}$, $\hat{B}$, $\hat{C}$, and $\hat{D}$ depend on the spin and parities associated with the particular contributions considered. Detailed expressions for these operators are given in the Appendix.

Equation (49) can be either evaluated directly or converted to the equivalent Pauli form,

$$\begin{aligned} &\bar{u}_{M_\Lambda}(p_\Lambda)\hat{T}u_{M_p}(p_p) \\ &\quad = N_\Lambda N_p \chi^\dagger_{M_\Lambda}[(\hat{A}+\hat{C})+(\hat{B}+\hat{D})\sigma\cdot\hat{p}_p \\ &\qquad +\sigma\cdot\hat{p}_\Lambda(\hat{D}-\hat{B})+\sigma\cdot\hat{p}_\Lambda(\hat{C}-\hat{A})\sigma\cdot\hat{p}_p]\chi_{M_p}, \end{aligned} \tag{50}$$

where

$$N = \sqrt{\frac{E+m}{2m}} \tag{51}$$

and

$$\hat{p} = \frac{\mathbf{p}}{E+m}. \tag{52}$$

The Pauli matrix elements can be evaluated analytically, but the procedure is tedious. Instead, we have evaluated Eq. (50) numerically. As a check on the procedure, an independent code was written to evaluate the Dirac matrix elements numerically without recourse to the Pauli reduction given by Eq. (50), and the results were compared with those of the numerical evaluation of Eq. (50).

III. DETAILS OF THE FITTING PROCEDURE

Table I lists the s- and u-channel resonances with three- or four-star status in the particle data tables [35] that are included in our fits.

On-shell branching ratios for the s-channel (nucleon) resonances included in Table I are given in Table II. Where data exist, the values appearing in the table are the averages of the values given in the most recent particle data tables [35]. It should be noted that these values differ somewhat from those used in Ref. [27] because in that earlier reference, data from earlier particle data tables were employed that differ somewhat from the data in the most recent tables. After summing the branching ratios obtained from the particle data tables, any remaining decay width still not accounted for was assigned to whatever other channels were open for that resonance. For the two-body decay channels, these assignments were guided in part by SU(3)-symmetry relations. Previous work by one of our authors indicates that the numerical results are not strongly sensitive to the details of the dynamical width model employed, provided that the total widths are normalized to the empirical width on-shell. The reader should consult Ref. [26] for details.

TABLE I. Well-established resonances considered in the model.

Resonance	I	J^P
$N(1440)$	$\frac{1}{2}$	$\frac{1}{2}^+$
$N(1520)$	$\frac{1}{2}$	$\frac{3}{2}^-$
$N(1535)$	$\frac{1}{2}$	$\frac{1}{2}^-$
$N(1650)$	$\frac{1}{2}$	$\frac{1}{2}^-$
$N(1675)$	$\frac{1}{2}$	$\frac{5}{2}^-$
$N(1680)$	$\frac{1}{2}$	$\frac{5}{2}^+$
$N(1700)$	$\frac{1}{2}$	$\frac{3}{2}^-$
$N(1710)$	$\frac{1}{2}$	$\frac{1}{2}^+$
$N(1720)$	$\frac{1}{2}$	$\frac{3}{2}^+$
$\Lambda(1405)$	0	$\frac{1}{2}^-$
$\Lambda(1520)$	0	$\frac{3}{2}^-$
$\Lambda(1600)$	0	$\frac{1}{2}^+$
$\Lambda(1670)$	0	$\frac{1}{2}^-$
$\Lambda(1690)$	0	$\frac{3}{2}^-$
$\Lambda(1810)$	0	$\frac{1}{2}^+$
$\Lambda(1820)$	0	$\frac{5}{2}^+$
$\Lambda(1830)$	0	$\frac{5}{2}^-$
$\Lambda(1890)$	0	$\frac{3}{2}^+$
$\Lambda(2110)$	0	$\frac{5}{2}^+$
$\Sigma(1385)$	1	$\frac{3}{2}^+$
$\Sigma(1660)$	1	$\frac{1}{2}^+$
$\Sigma(1670)$	1	$\frac{3}{2}^-$
$\Sigma(1750)$	1	$\frac{1}{2}^-$
$\Sigma(1775)$	1	$\frac{5}{2}^-$
$\Sigma(1915)$	1	$\frac{5}{2}^+$
$\Sigma(1940)$	1	$\frac{3}{2}^-$

TABLE II. On-shell $N^\star$ branching ratios.

Resonance	Two-body channels			Three-body channels		
	$N\pi$	$N\eta$	ΛK	$N\sigma$	$\Delta(1232)\pi$	$N\rho$
$N(1440)$	0.65			0.075	0.25	0.025
$N(1520)$	0.60				0.20	0.20
$N(1535)$	0.44	0.515		0.02		0.025
$N(1650)$	0.77	0.06	0.07		0.03	0.07
$N(1675)$	0.40				0.6	
$N(1680)$	0.60			0.15	0.125	0.125
$N(1700)$	0.10				0.80	0.10
$N(1710)$	0.15	0.06	0.14	0.25	0.26	0.14
$N(1720)$	0.15	0.04	0.06			0.75

In addition to the resonances listed in Table I, four additional nucleon resonances, which have two-star status in the particle data tables, were included. These are listed in Table III.

These higher mass s-channel resonances were included to improve the fits to the data at the higher energy end of the kinematic region considered. Aside from the empirical evidence for their existences, as reflected in their particle data table listings, they are predicted by quark models [36], and some of them have been included in another recent analysis of photoproduction data [29]. In accord with our philosophy to incorporate only resonances for which there is independent empirical evidence, we have *not* included the so-called "missing" $\frac{3}{2}^-$ resonance at 1900 MeV in our final results. Although this resonance has been predicted in quark models [36] and has been included in several other analyses of strangeness photoproduction [18,24,29], there has so far been little evidence for its existence in any other reactions. We will comment on this further in Sec. IV.

As discussed, width data for the resonances listed in Table III are extremely limited or nonexistent. For this reason, no attempt has been made to extend our dynamical off-shell width model to these resonances. Instead, their widths are treated as energy-independent parameters to be determined in the fits to the data. The complete set of varied parameters thus includes the coupling strength products in all three channels and the total widths of the resonances in Table III. The coupling strength products are defined by the relations

$$\begin{aligned} F_{N^\star} &= e\kappa_{pN^\star} g_{\Lambda K N^\star}, \\ F_{\Lambda^\star} &= e\kappa_{\Lambda\Lambda^\star} g_{\Lambda^\star K p}, \\ F_{\Sigma^\star} &= e\kappa_{\Lambda\Sigma^\star} g_{\Sigma^\star K p} \end{aligned} \tag{53}$$

TABLE III. Two-star nucleon resonances considered in the model.

Resonance	J^P
$N(1900)$	$\frac{3}{2}^+$
$N(2000)$	$\frac{5}{2}^+$
$N(2080)$	$\frac{3}{2}^-$
$N(2200)$	$\frac{5}{2}^-$

for the ground-state baryons and spin $\frac{1}{2}$ resonances in the s and u channels, by

$$\begin{aligned} G^1_{N^\star} &= g_1^{pN^\star} g_{\Lambda K N^\star}, \\ G^2_{N^\star} &= g_2^{pN^\star} g_{\Lambda K N^\star}, \\ G^1_{\Lambda^\star} &= g_1^{\Lambda\Lambda^\star} g_{\Lambda^\star K p}, \\ G^2_{\Lambda^\star} &= g_2^{\Lambda\Lambda^\star} g_{\Lambda^\star K p}, \\ G^1_{\Sigma^\star} &= g_1^{\Lambda\Sigma^\star} g_{\Sigma^\star K p}, \\ G^2_{\Sigma^\star} &= g_2^{\Lambda\Sigma^\star} g_{\Sigma^\star K p} \end{aligned} \tag{54}$$

for the spin $\frac{3}{2}$ and spin $\frac{5}{2}$ resonances in the s and u channels, by

$$F_K = -e g_{\Lambda K p} \tag{55}$$

for the ground-state kaon in the t channel, and by

$$\begin{aligned} G^V_{K^\star} &= g_{\gamma K K^\star} g^V_{\Lambda K^\star p}, \\ G^T_{K^\star} &= g_{\gamma K K^\star} g^T_{\Lambda K^\star p} \end{aligned} \tag{56}$$

for the t-channel kaon resonances, where $e = 0.3029$ is the dimensionless electric charge. Note in Eqs. (53) that the $N^\star$, $\Lambda^\star$, and $\Sigma^\star$ subscripts refer to either the corresponding ground-state baryon or a spin $\frac{1}{2}$ resonance. For the proton, we also need the charge-coupling product. This is given by

$$F_{Cp} = e g_{\Lambda K p}. \tag{57}$$

The various Born term coupling products can be related to each other through SU(3)-symmetry relations, SU(2) isospin coupling coefficients, and the well-established values for the Baryon ground-state magnetic moments. In particular, F_p, F_Λ, F_K, and F_{Cp} satisfy the simple relationships

$$\begin{aligned} F_p &= \kappa_p F_{Cp}, \\ F_\Lambda &= \kappa_\Lambda F_{Cp}, \\ F_K &= -F_{Cp}. \end{aligned} \tag{58}$$

For the magnetic moment factors in these relations, we employ the values [35] $\kappa_p = -1.79$ and $\kappa_\Lambda = -0.729$ [note the definitions of the κ's as given by Eqs. (13) and (14)].

The two strong coupling strengths, $g_{\Lambda K p}$ and $g_{\Sigma K p}$, each can be expressed as a product of an SU(3) isoscalar factor and an SU(2) Clebsch-Gordon coefficient,

$$\begin{aligned} g_{\Lambda K p} &= \left(00\tfrac{1}{2}\tfrac{1}{2}\middle|\tfrac{1}{2}\tfrac{1}{2}\right) f_{\Lambda K N}, \\ g_{\Sigma K p} &= \left(10\tfrac{1}{2}\tfrac{1}{2}\middle|\tfrac{1}{2}\tfrac{1}{2}\right) f_{\Sigma K N}. \end{aligned} \tag{59}$$

The SU(3) isoscalar factors appearing here are related by SU(3) symmetry [37]. In particular, their ratio can be expressed in terms of an SU(3) parameter α,

$$\frac{f_{\Sigma K N}}{f_{\Lambda K N}} = -\frac{1-2\alpha}{1-\frac{2}{3}\alpha}, \tag{60}$$

which, in turn, can be fixed by other couplings within the same SU(3) multiplets. Using the empirical values for the couplings of pions to the Σ and Λ baryons [38] yields the value $\alpha = 0.625$. Combining Eqs. (59) and (60) with the coupling product definitions, Eq. (53), we obtain the ratio

$$\frac{F_\Sigma}{F_\Lambda} = \frac{1}{\sqrt{3}} \frac{1-2\alpha}{1-\frac{2}{3}\alpha} \frac{\kappa_\Lambda}{\kappa_{\Lambda\Sigma}}. \tag{61}$$

For the transition magnetic moment parameter, we use the particle data table value [35], $\kappa_{\Lambda\Sigma} = 1.91$, to get $\frac{F_\Sigma}{F_\Lambda} = 0.647$. The imposition of these relations reduces the number of Born parameters to be varied to just one, which we choose to be the parameter F_{Cp}.

The parameter F_{Cp} is also restricted by SU(3)-symmetry relations and by other considerations. A recent study by General and Cotanch [39] based on a generalized Goldberger-Treiman relation in conjunction with the Dashen-Weinstein sum rule arrived at the pair of constraints, $0.80 \leqslant \frac{g_{K\Sigma N}}{\sqrt{4\pi}} \leqslant 2.72$ and $-3.90 \leqslant \frac{g_{K\Lambda N}}{\sqrt{4\pi}} \leqslant -1.84$. The second constraint yields an upper limit for F_{Cp} of -1.98. Because the photoproduction data, analyzed within the model presented here, seem to favor a small magnitude for F_{Cp}, we use this upper limit in the first of our fits, which has F_{Cp} fixed. For the second fit, we allowed F_{Cp} to assume whatever value yields the best fit to the data consistent with the Born term relations given earlier. Comparison of the two fits enabled us to study the extent to which the quality of the fit is affected by the constraint on F_{Cp}. Note that the choice $F_{Cp} = -1.98$ yields the value $F_\Sigma = 0.934$, which is consistent with General and Cotanch's constraint on the value of $g_{K\Sigma N}$.

The fitting procedure required many iterations starting with a fit of the most recent CLAS data [10] for the unpolarized differential cross section, given in the CM by

$$\frac{d\sigma}{d\Omega} = \frac{1}{(2\pi)^2} \frac{m_p m_\Lambda p_F}{4 E_\gamma s} \frac{1}{4} \sum_{\text{spins}} |\langle F|\hat{T}|I\rangle|^2, \tag{62}$$

where p_F is the outgoing three-momentum in the CM and $s = W^2$ is the squared CM energy. The resulting parameter values were then employed as starting values to fit the cross-section data, the CLAS [8], SAPHIR [4], and GRAAL [9] data for the hyperon polarization asymmetry P, and the CLAS [11] data for the double-polarization observables C_x and C_z. Here, P is defined by

$$P = \frac{d\sigma^+_\Lambda - d\sigma^-_\Lambda}{d\sigma^+_\Lambda + d\sigma^-_\Lambda}, \tag{63}$$

where the superscripts $^+$ and $^-$ refer to spin projections above and below the scattering plane and C_x and C_z are defined by

$$C_{i'} = \frac{d\sigma^+_\Lambda - d\sigma^-_\Lambda}{d\sigma^+_\Lambda + d\sigma^-_\Lambda}, \tag{64}$$

where now the superscripts $^+$ and $^-$ refer to Λ spin projections along and opposite to the $i = z$ or $i = x$ axes and the incident photon is circularly polarized with positive helicity.

At this juncture we used the model to calculate the photon-beam asymmetry prior to including it in the fit. The photon-beam asymmetry is defined by the relation

$$\Sigma = \frac{d\sigma^\perp_\Lambda - \sigma^\parallel_\Lambda}{d\sigma^\perp_\Lambda + \sigma^\parallel_\Lambda}, \tag{65}$$

where $\perp$ and $\parallel$ refer to polarization vectors perpendicular and parallel to the scattering plane, respectively. Our results gave good agreement with the GRAAL [9] data for this observable if we interpreted their definition of Σ to be the negative of the one defined earlier. Our definition is the standard one used in most theoretical analyses. The GRAAL definition is given in terms of vertical and horizontal planes that are not specified relative to the scattering plane, so the possibility exists that there is a sign discrepancy between our definition of Σ and that of the experimentalists. The definition of Σ employed by the LEPS collaboration seems to agree with the GRAAL definition. In any case, we then completed the fitting procedure by incorporating both the GRAAL and the LEPS [5] Σ data in the fit with the sign of Eq. (65) reversed.

In carrying out the fits, we minimized the χ^2 per degree of freedom defined by the relation

$$\frac{\chi^2}{\nu} = \sum \frac{(Y_{\text{calc}} - Y_{\text{exp}})^2}{\sigma^2}, \tag{66}$$

where the sum is over all individual data points, Y_{calc} and Y_{exp} are the calculated and experimental values of the observable, and σ^2 is the squared statistical uncertainty in Y_{exp}. The number of degrees of freedom is given by $\nu = N_{\text{data}} - N_{\text{par}}$, where N_{data} is the number of data points and N_{par} is the number of parameters in the fit.

A code based on a modified Marquardt prescription was employed in the fitting procedure. As well as the parameters themselves, this code generates the covariance matrix associated with the fit from which well-defined parameter uncertainties can be extracted.

IV. NUMERICAL RESULTS AND DISCUSSION

The parameters from the fit with all of the Born terms constrained (the first fit described in the previous section) are presented in Table IV. Here the coupling constant products obtained for all resonances included in the final fit are listed together with the total widths obtained for the higher mass nucleon resonances included. Listed also are the parameter uncertainties obtained from the covariance matrix of the fit. These uncertainties measure the sensitivities of the fit to the corresponding parameters. A small relative value for this uncertainty means that the corresponding parameter is well determined by the fit; by contrast, a large relative value means that the parameter is poorly determined and is probably strongly correlated with other parameters in the fit. The χ^2 per degree of freedom associated with this fit is 1.68.

We have not listed the parameters obtained in the second fit in which the parameter F_{Cp} was allowed to vary because they are very similar to those obtained in the fit in which F_{Cp} was fixed at -1.98. In fact, with the exception of F_{Cp}, the differences in the parameters obtained in the two fits all lie within the parameter uncertainties derived from the covariance matrices. As mentioned, the values obtained for the χ^2 per degree of freedom in the two fits differ by less than 1%, and the results obtained for the observables are nearly indistinguishable. In the second fit, the value obtained for F_{Cp} increased to the value -1.71 with an uncertainty of 0.13—nearly within 1 standard deviation of the upper limit.

TABLE IV. Fit results. In this fit, the Born parameter F_{Cp} was fixed at the value of -1.98. The width values are given in MeV.

	Spin $\frac{1}{2}$ resonances	
$N(1440)$	$F_{N^\star}$	4.839 ± 0.224
$N(1535)$	$F_{N^\star}$	0.130 ± 0.027
$N(1650)$	$F_{N^\star}$	0.100 ± 0.012
$N(1710)$	$F_{N^\star}$	0.0008 ± 0.011
$\Lambda(1405)$	$F_{\Lambda^\star}$	3.43 ± 5.10
$\Lambda(1670)$	$F_{\Lambda^\star}$	-8.70 ± 6.51
	Spin $\frac{3}{2}$ resonances	
$N(1520)$	$G^1_{N^\star}$	0.370 ± 0.090
	$G^2_{N^\star}$	-0.067 ± 0.128
$N(1700)$	$G^1_{N^\star}$	-0.453 ± 0.052
	$G^2_{N^\star}$	-0.391 ± 0.067
$N(1720)$	$G^1_{N^\star}$	-0.105 ± 0.004
	$G^2_{N^\star}$	-0.200 ± 0.013
$N(1900)$	$G^1_{N^\star}$	-0.051 ± 0.003
	$G^2_{N^\star}$	-0.050 ± 0.008
	Γ	258.6 ± 9.8
$N(2080)$	$G^1_{N^\star}$	0.006 ± 0.004
	$G^2_{N^\star}$	0.003 ± 0.003
	Γ	65.5 ± 21.4
$\Lambda(1890)$	$G^1_{\Lambda^\star}$	-4.90 ± 0.59
	$G^2_{\Lambda^\star}$	5.12 ± 4.72
$\Sigma(1385)$	$G^1_{\Sigma^\star}$	1.728 ± 0.414
	$G^2_{\Sigma^\star}$	-2.14 ± 3.09
$\Sigma(1940)$	$G^1_{\Sigma^\star}$	0.128 ± 0.341
	$G^2_{\Sigma^\star}$	-1.098 ± 0.714
	Spin $\frac{5}{2}$ resonances	
$N(1675)$	$G^1_{N^\star}$	0.0069 ± 0.0004
	$G^2_{N^\star}$	0.0272 ± 0.0014
$N(1680)$	$G^1_{N^\star}$	-0.0104 ± 0.0040
	$G^2_{N^\star}$	0.0196 ± 0.0057
$N(2000)$	$G^1_{N^\star}$	-0.0130 ± 0.0069
	$G^2_{N^\star}$	-0.0272 ± 0.0127
	Γ	1133 ± 490
$N(2200)$	$G^1_{N^\star}$	-0.0009 ± 0.0003
	$G^2_{N^\star}$	-0.0035 ± 0.0010
	Γ	371.4 ± 91.5
$\Lambda(1820)$	$G^1_{\Lambda^\star}$	0.388 ± 0.170
	$G^2_{\Lambda^\star}$	0.170 ± 1.447
$\Lambda(1830)$	$G^1_{\Lambda^\star}$	-0.555 ± 0.075
	$G^2_{\Lambda^\star}$	1.151 ± 0.390
$\Lambda(2110)$	$G^1_{\Lambda^\star}$	0.127 ± 0.120
	$G^2_{\Lambda^\star}$	-0.181 ± 0.989
$\Sigma(1775)$	$G^1_{\Sigma^\star}$	0.517 ± 0.072
	$G^2_{\Sigma^\star}$	-1.083 ± 0.375
$\Sigma(1915)$	$G^1_{\Sigma^\star}$	-0.526 ± 0.287
	$G^2_{\Sigma^\star}$	-0.047 ± 2.420
	t-channel resonances	
$K(892)$	$G^V_{K^\star}$	1.090 ± 0.137
	$G^T_{K^\star}$	-2.325 ± 0.338
$K(1270)$	$G^V_{K^\star}$	3.074 ± 0.329
	$G^T_{K^\star}$	3.275 ± 1.350

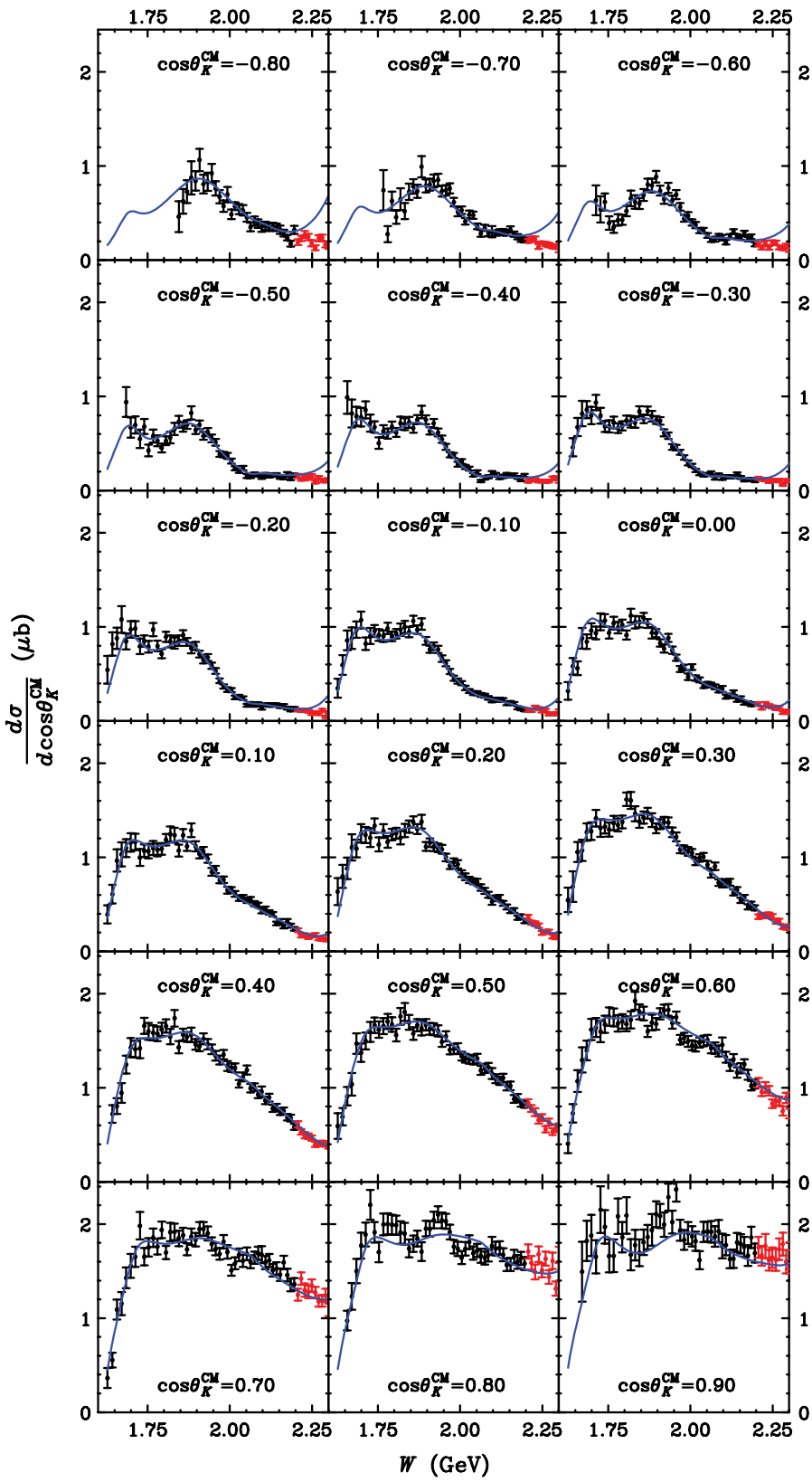

FIG. 2. (Color online) Differential cross sections vs. W for bins of $\cos\theta_K^{\rm CM}$ as indicated. Data above 2.2 GeV (red points) were not included in the fit. The curve is from our fit, and the data are from Ref. [10].

Several observations are in order concerning the contents of Table IV. First, it will be noted that the number of hyperon resonances appearing in this table is much smaller than the number appearing in Table I. We found that attempts to incorporate all of the hyperon resonances listed in Table I resulted in unacceptably large coupling products for many of these resonances accompanied by enormous parameter uncertainties. This clearly indicates that a model that

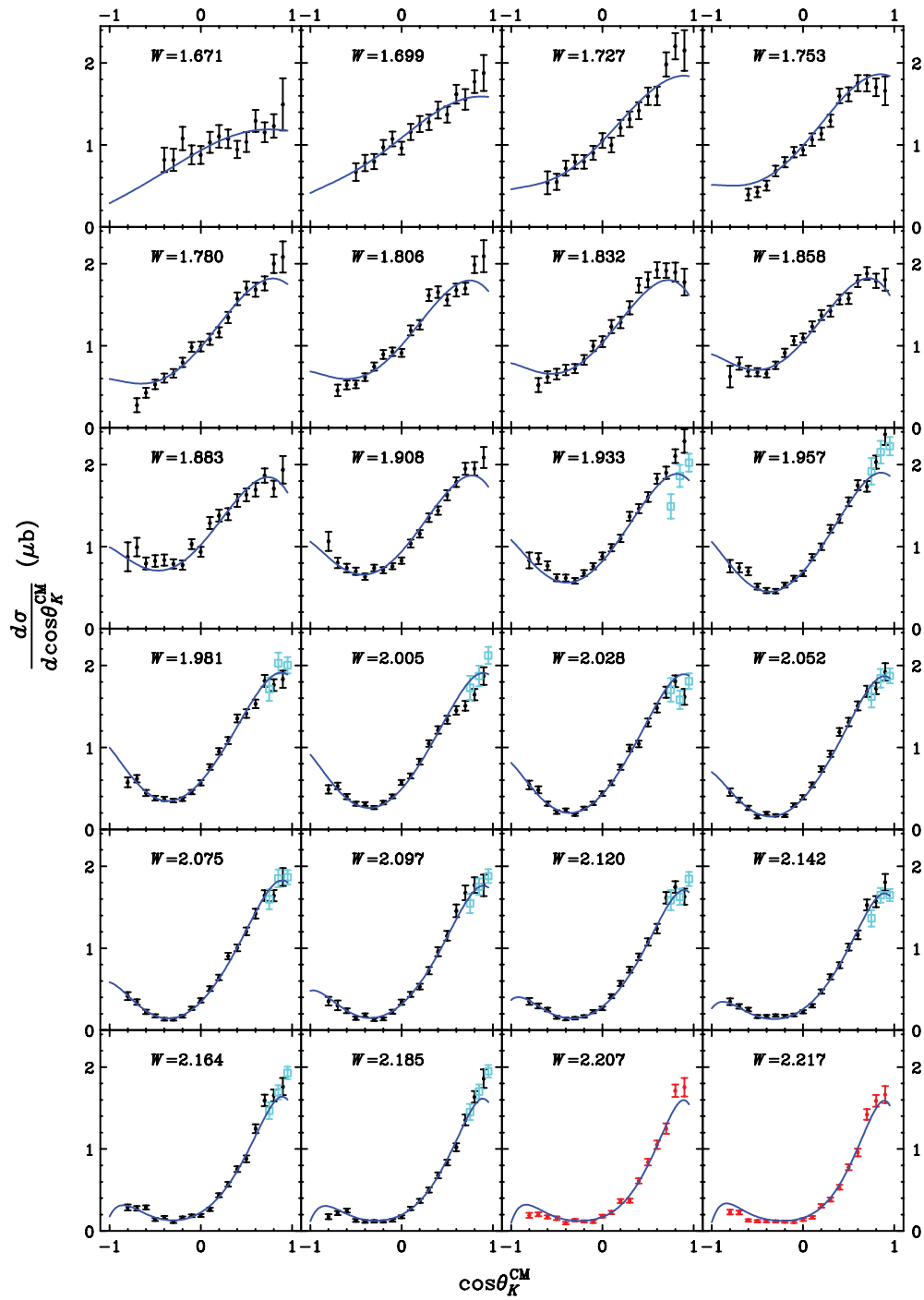

FIG. 3. (Color online) Differential cross-section vs. $\cos\theta_K^{\rm CM}$ for bins of W as indicated. The curve is from our fit. The data are from CLAS [10] (black points) and LEPS [5] (light-blue boxes). Note that the LEPS data are included here only for comparison purposes; they were note included in the fitting procedure. The highest two W bins are CLAS data that were not included in the fit.

incorporates all of the possible u-channel resonances is too rich (i.e., the photoproduction reaction is not sensitive to particular u-channel contributions and, thus, cannot be used to unambiguously determine individual u-channel coupling products). The reason for this is obvious once one notes that the kinematic variable u in the photoproduction reaction is usually negative. This makes the denominators of the intermediate baryon propagators in the u channel always large in magnitude and insensitive to the baryon mass. Thus, individual contributions to the reaction amplitude in the u channel are difficult to distinguish from one another and become highly correlated because many different combinations of the u-channel coupling products yield the same result in the reaction matrix element. Two consequences of this are very large parameter uncertainties and the possibility of a runaway effect in the fitting routine in which small increases

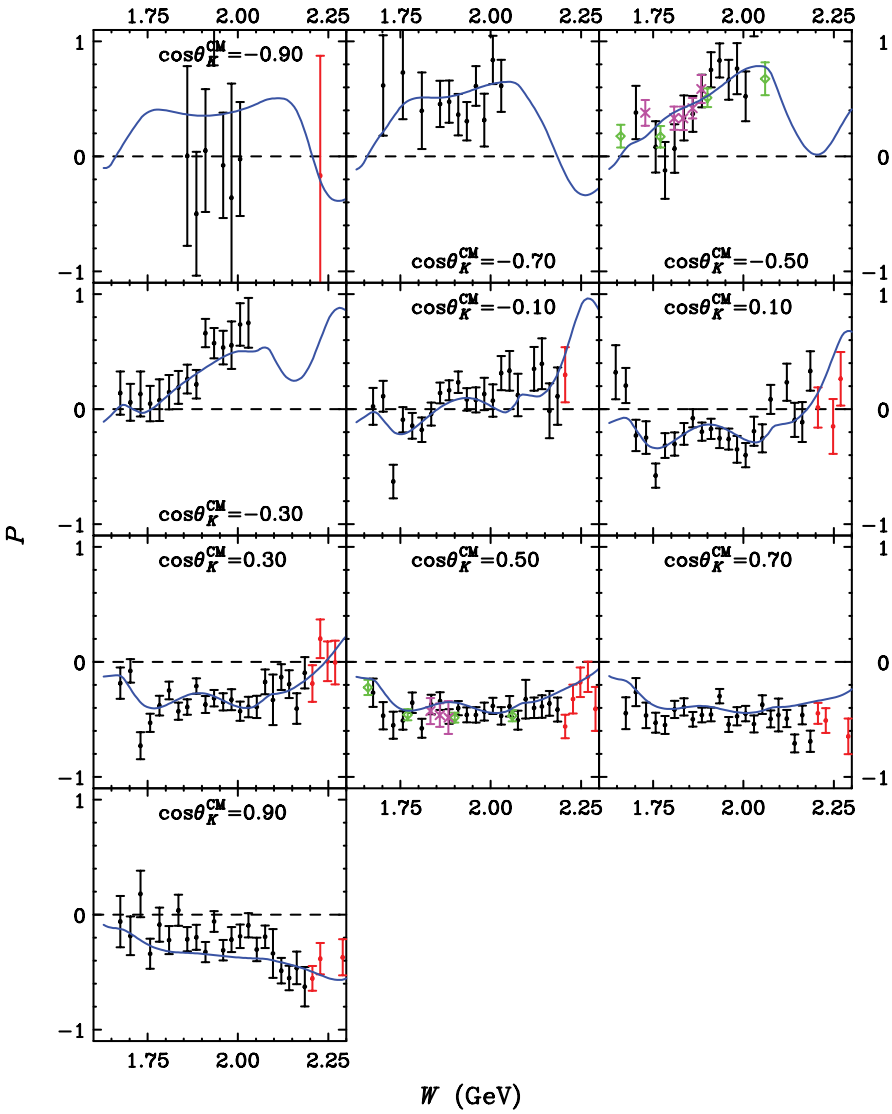

FIG. 4. (Color online) Λ polarization, P, vs. W for bins of $\cos\theta_K^{\rm CM}$ as indicated. Data above 2.2 GeV were not included in the fit. The curve is from our fit to data from CLAS [8] (black points), GRAAL [9] (pink crosses), and SAPHIR [4] (green diamonds).

in χ^2/ν result from simultaneous huge increases in correlated couplings.

To avoid this difficulty, we systematically removed those u-channel resonances with the largest parameter uncertainties and then refit the remaining parameters, accepting the result if the resulting χ^2/ν did not increase by more than a few percent over the value obtained with all resonances included. This procedure led to reduced values of the remaining u-channel coupling products and greatly reduced parameter uncertainties, finally culminating in the values listed in Table IV. Attempts to further reduce the number of u-channel resonances incorporated in the model led to larger increases in χ^2/ν (10% or more) than we deemed acceptable. As the procedure was carried out, the values obtained for the s- and t-channel coupling products did not shift significantly, indicating that these coupling products are not sensitive to the model employed for the u channel.

Even with the reduction in the number of u-channel resonances included in the fit, the parameter uncertainties associated with the hyperon resonances are still rather large, often larger than the magnitudes of the couplings themselves. This indicates that the u-channel couplings are still highly correlated and poorly determined. Evidently, the photoproduction reaction is of limited value as a means for studying the couplings of hyperon resonances.

The quality of our fits is illustrated in Figs. 2–6. Figure 2 shows the W dependence of the differential cross section for different values of $\cos\theta_K^{\rm CM}$. Over the range in W that the data were fit (up to 2.2 GeV), our fit well reproduces the features of the data. The minor exception is in the two forward-angle bins at around $W \sim 1900$ GeV, where the data show a peak not indicated by our fit. This could well be an indication of the presence of the $D_{13}(1900)$ included by others [18,24,29]. Figure 3 shows the same cross section plotted against $\cos\theta_K^{\rm CM}$ for a selection of W values. This figure also includes data from LEPS, but only the CLAS cross-section data were used in the generation of the fit.

Our model actually does a good job of matching the cross-section data up to $W \sim 2.3$ GeV for forward angles, which is a trend seen for the other observables as well.

The Λ-polarization fits are shown as a function of W in Fig. 4 and as a function of $\cos\theta_K^{\rm CM}$ for selected W bins in

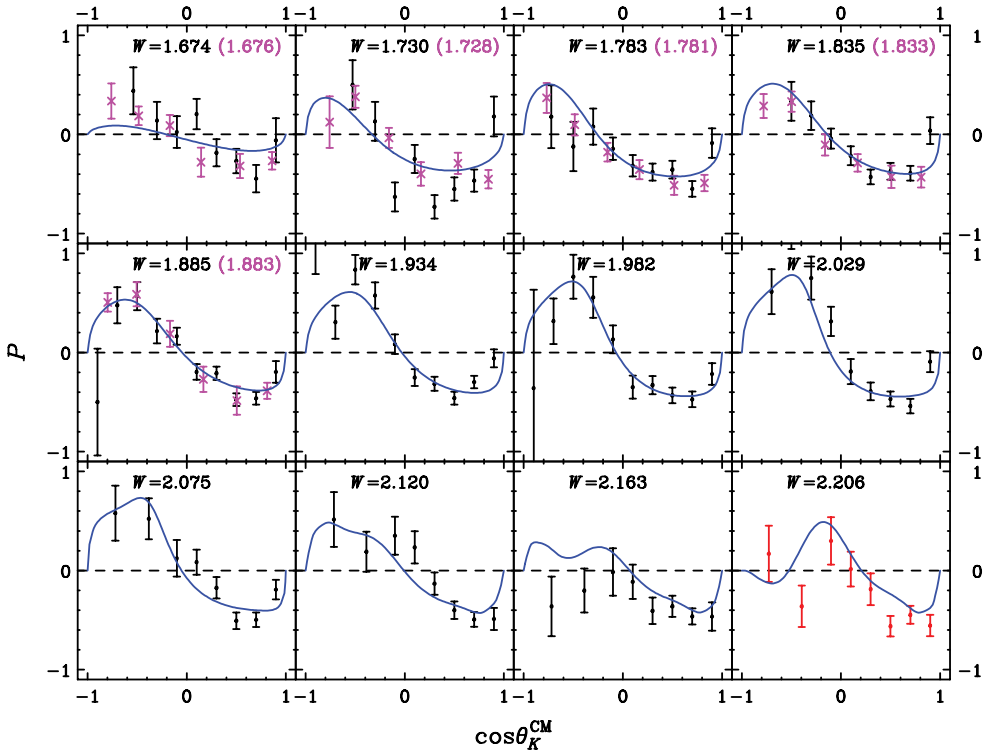

FIG. 5. (Color online) Λ polarization, P, vs. $\cos\theta_K^{\rm CM}$ for bins of W as indicated. The curve is from our fit and data are from CLAS [8] (black points) and SAPHIR [4] (pink crosses) with a similar value of W, which is indicated in the parentheses.

Fig. 5. As with the cross section, our fit reproduces the major features of the data quite well.

Figure 6 shows the photon-beam asymmetry Σ as a function of $\cos\theta_K^{\rm CM}$. The fit shows excellent agreement with the GRAAL data ($W \leqslant 1.906$ GeV). However, from $W = 1.947$ GeV up to 2.2 GeV, disagreement between these LEPS data and the fit grows with W.

Figures 7 and 8 show the fits of the C_x data. Over most of the kinematic range of data, we again reproduce the general features of the data with our fit. The exception here is at low W (see especially Fig. 8, panel $W = 1.679$ GeV), where the data are systematically lower than our fit.

Figures 9 and 10 show the fits of the C_z data. In the two most forward-angle bins of the W distributions, the fit is systematically lower than the data from about 1.9 to 2.1 GeV. Otherwise, the data are well represented by the fit.

Detailed examination of the matrix elements in the model reveals that the s-channel matrix elements, u-channel matrix elements, and t-channel matrix elements, when taken individually, all increase monotonically with energy. This indicates that successful reproduction of the data results from a subtle interference between the matrix elements in different channels. Because the Mandelstam variables u and t are generally negative over the energy range of interest here, the individual resonance contributions in the u and t channel are only weakly dependent on the energy. By contrast, the individual s-channel contributions are strongly energy dependent, especially at energies near the resonance masses. Consequently, to successfully fit the data within a given energy range with reasonable parameter values, it is necessary to include nucleon resonances with masses that span the full energy range considered. Because only nucleon resonances with masses up to 2.2 GeV were included in the fits, attempts to fit the data beyond 2.2 GeV resulted in a χ^2/ν that increased rapidly with W. Furthermore, because of the subtle interferences among the three channels that are fine-tuned by the fit, fits obtained within a given range of energies cannot be extended significantly beyond that range. Indeed, one finds that beyond the energy range of the fit, the calculated cross sections increase precipitously with energy, in marked contrast with the data.

In summary, we have presented a new fit of the kaon photoproduction data from a variety of sources using an effective Lagrangian model. In this fit, the Born terms were all fixed at values imposed by SU(3)-symmetry constraints and other considerations. A second fit, in which the value of the Born parameter F_{Cp} was allowed to vary while requiring the other Born parameters to satisfy SU(3) relations among the various Born couplings, did not differ significantly from the first fit. In both fits, data for the unpolarized cross section, the hyperon polarization asymmetry, photon-beam asymmetry, and two double-polarization observables from threshold up to 2.2 GeV were included.

In general, the new fit yields good representations of both the cross-section data and the spin observables. One exception is the forward-angle cross-section data around 1.9 GeV. This suggests that our fit is perhaps missing one or more resonances in this energy range, which is a subject for future work. Further improvements to our model should result from including other polarization observables. The CLAS

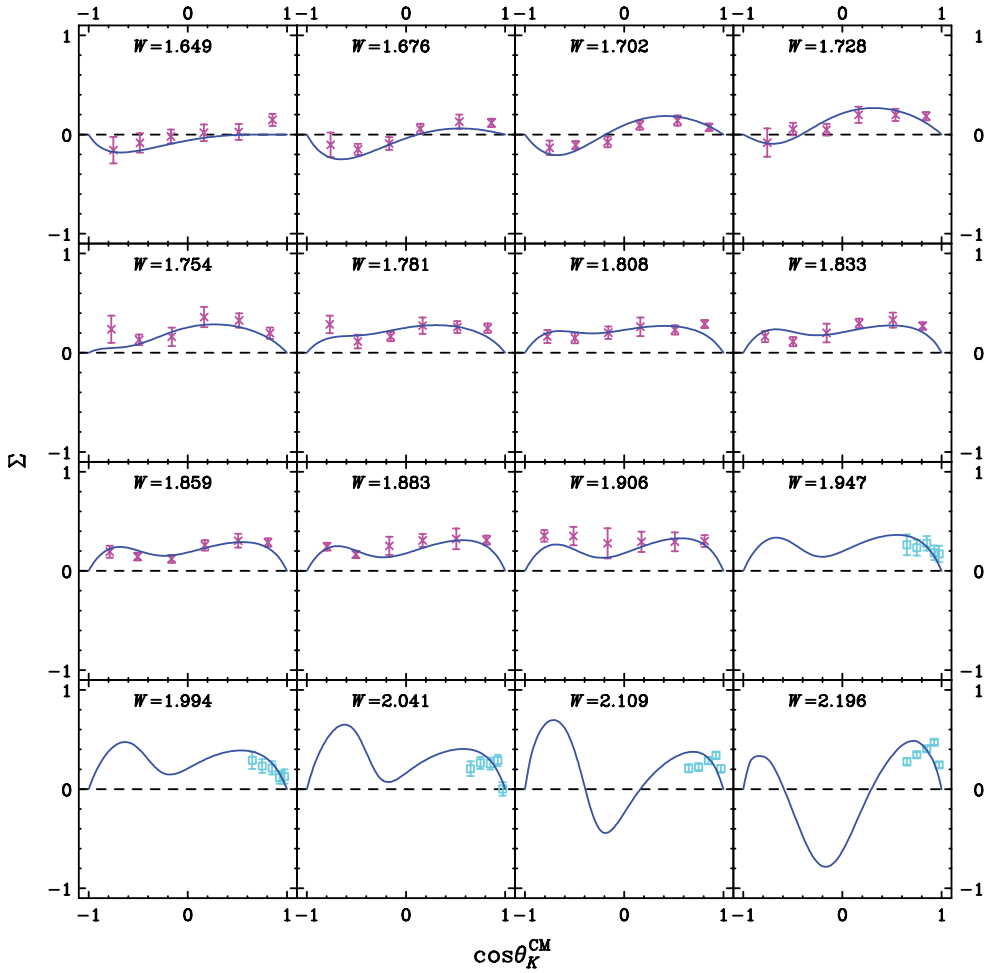

FIG. 6. (Color online) Σ vs. $\cos\theta_K^{\rm CM}$ for bins of W as indicated. The curve is from our fit and the data are from GRAAL [9] (pink crosses) and LEPS [5] (light-blue boxes).

collaboration expects to produce multiple spin observables in the near future [40], including data with a polarized target and a linearly polarized photon beam. Recently, the GRAAL Collaboration has published results for the double-polarization observables O_x and O_z [41]. Such data should provide more constraints and potentially enable inclusion of resonances that are not necessary in our fit.

The results of this work can be employed to study the electroproduction of kaons from the proton (i.e., the reaction $ep \to e'K^+\Lambda$). The latter reaction involves a virtual, rather than a real, photon in the strangeness production interaction and, thus, requires electromagnetic form factors at the photon vertices. If one uses the photoproduction fits described here to represent the underlying reaction mechanism in the electroproduction reaction, then one can use electroproduction data to study the electromagnetic form factors associated with the intermediate hadrons in the different reaction channels. Of course, the electroproduction reaction involves longitudinal, as well as transverse, photons, but the corresponding contributions to the reaction amplitude are related through the Lorentz structure of the interaction vertices (i.e., through the fact that the photon polarization vector is a Lorentz four-vector). Thus, it should be possible to extract important information concerning the electromagnetic form factors of hadronic resonances using the fits described here in conjunction with electroproduction data. Work in this direction is currently in progress.

APPENDIX: AMPLITUDE OPERATORS

The operators $\hat{A}$, $\hat{B}$, $\hat{C}$, and $\hat{D}$ appearing in Eqs. (49) and (50) depend on the spin and parity of the particular intermediate hadron considered. They can all be expressed in terms of a set of Σ and Ω operators defined by the relations

$$\begin{aligned} \Sigma(a,b) &= a_0 b_0 - \sigma\cdot\mathbf{a}\sigma\cdot\mathbf{b}, \\ \Omega(a,b) &= b_0\sigma\cdot\mathbf{a} - a_0\sigma\cdot\mathbf{b}, \end{aligned} \tag{A1}$$

$$\begin{aligned} \Sigma_3(a,b,c) &= a_0\Sigma(b,c) - \sigma\cdot\mathbf{a}\Omega(b,c), \\ \Omega_3(a,b,c) &= a_0\Omega(b,c) - \sigma\cdot\mathbf{a}\Sigma(b,c), \end{aligned} \tag{A2}$$

and

$$\begin{aligned} \Sigma_4(a,b,c,d) &= \Sigma(a,b)\Sigma(c,d) + \Omega(a,b)\Omega(c,d), \\ \Omega_4(a,b,c,d) &= \Sigma(a,b)\Omega(c,d) + \Omega(a,b)\Sigma(c,d), \end{aligned} \tag{A3}$$

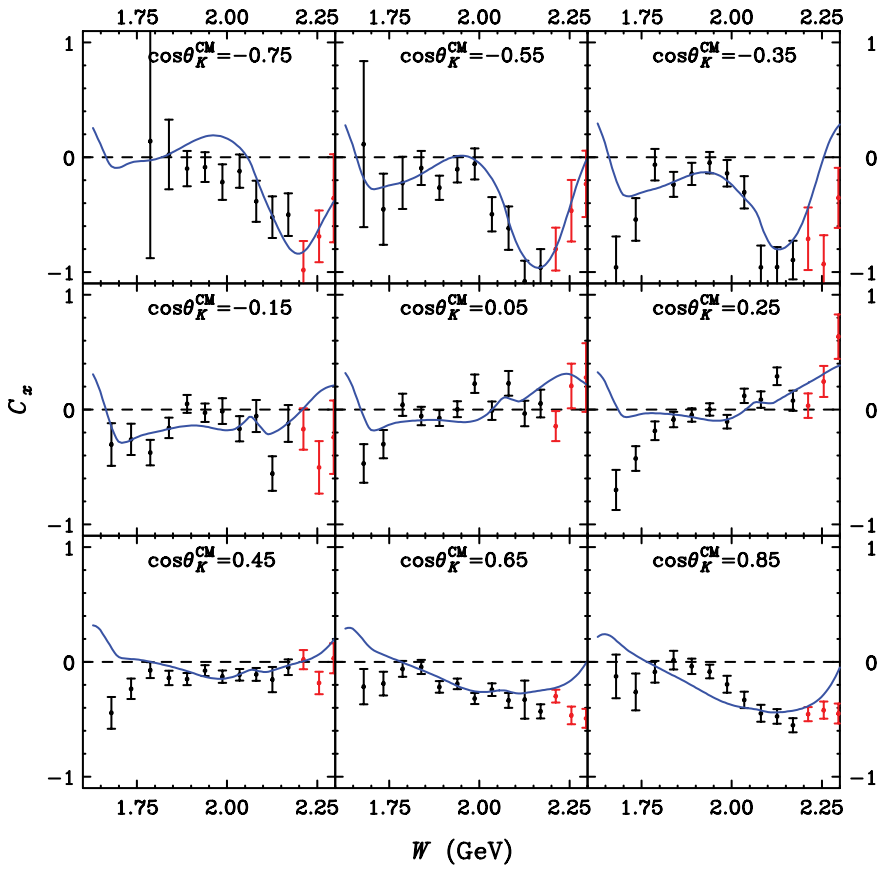

FIG. 7. (Color online) C_x vs. W for bins of $\cos\theta_K^{\rm CM}$ as indicated. Data above 2.2 GeV were not included in the fit. The curve is from our fit and data are from CLAS [11].

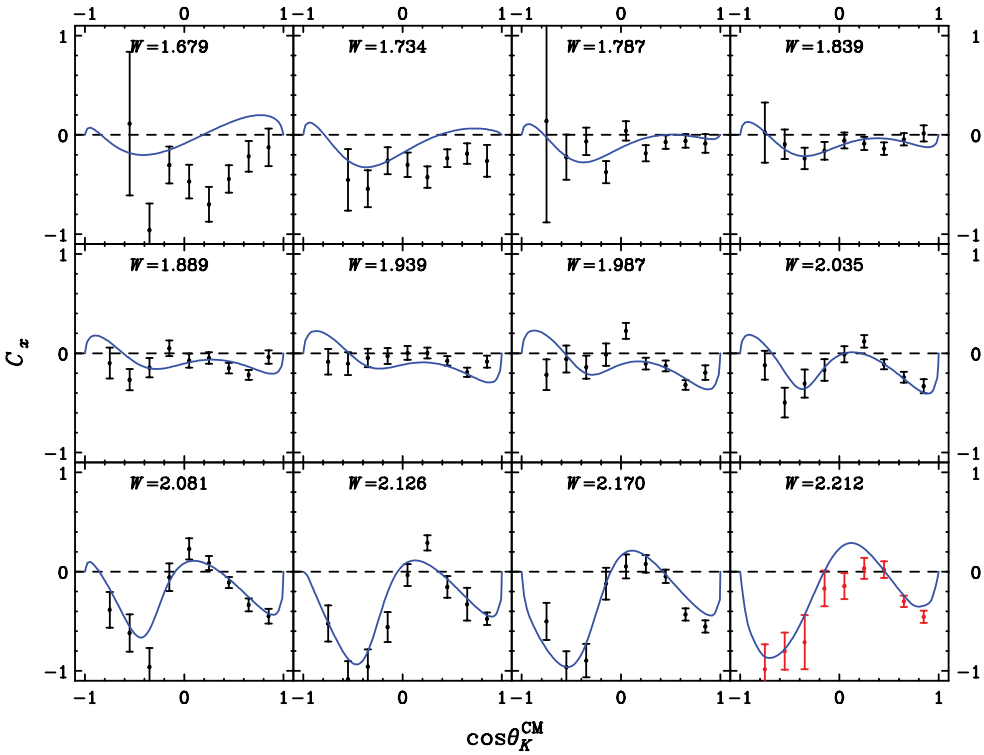

FIG. 8. (Color online) C_x vs. $\cos\theta_K^{\rm CM}$ for bins of W as indicated. The curve is from our fit and the data points are from CLAS [11]. The data in the highest W bin were not included in the fit.

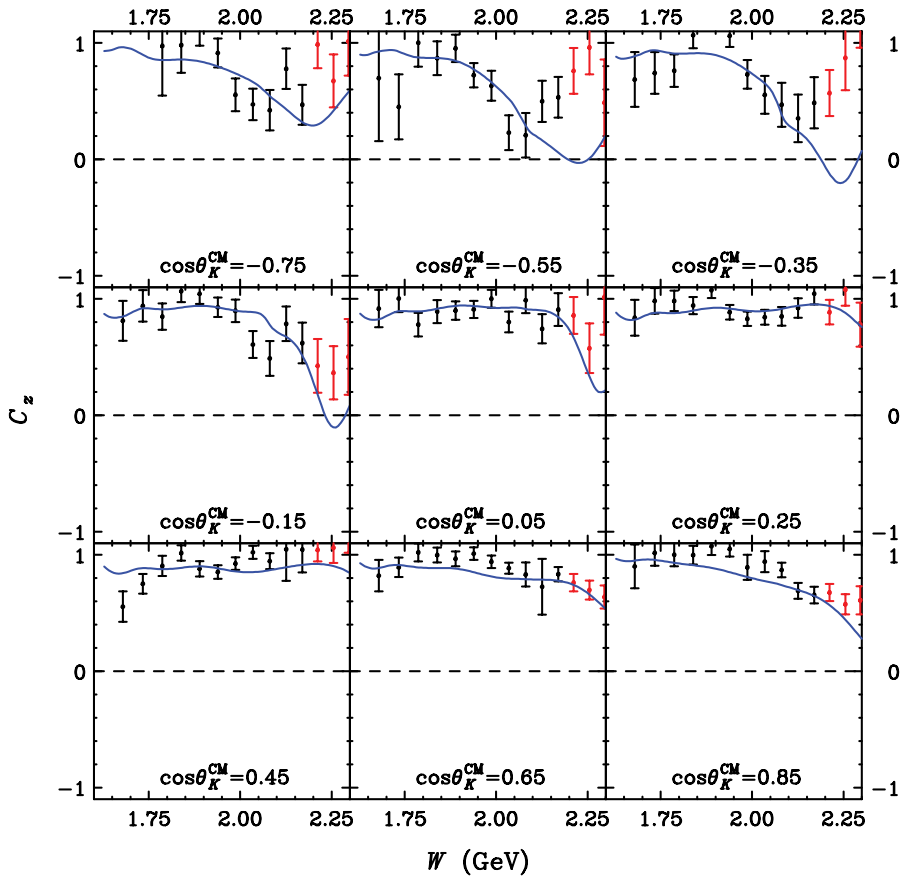

FIG. 9. (Color online) C_z vs. W for bins of $\cos\theta_K^{\rm CM}$ as indicated. Data above 2.2 GeV were not included in the fit. The curve is from our fit and data are from CLAS [11].

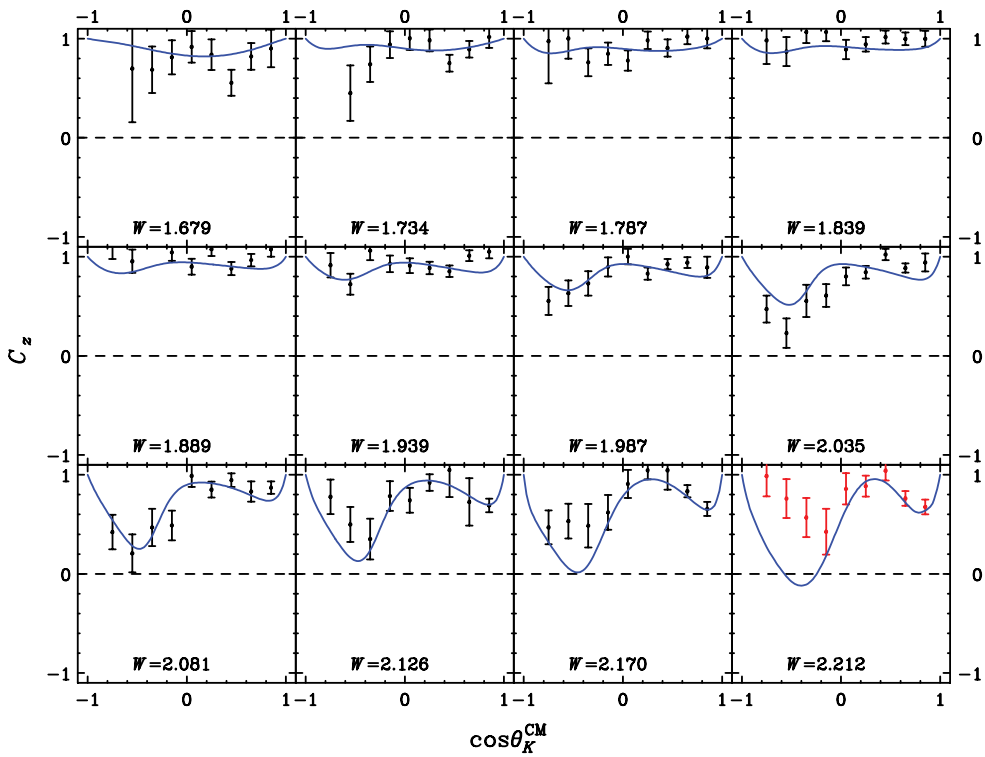

FIG. 10. (Color online) C_z vs. $\cos\theta_K^{\rm CM}$ for bins of W as indicated. The curve is from our fit and the data points are from CLAS [11]. The data in the highest W bin were not included in the fit.

where a_0 and $\mathbf{a}$ are the time and space components of the four-vector a. In terms of these operators, the operators for intermediate baryons with positive parity and spin $\frac{1}{2}$ are

$$\begin{aligned}\hat{A}_s^{\frac{1}{2}^+} &= FD(p)m\Omega(p_\gamma,\epsilon),\\ \hat{B}_s^{\frac{1}{2}^+} &= FD(p)m\Sigma(p_\gamma,\epsilon),\\ \hat{C}_s^{\frac{1}{2}^+} &= -FD(p)\Omega_3(p,p_\gamma,\epsilon),\\ \hat{D}_s^{\frac{1}{2}^+} &= -FD(p)\Sigma_3(p,p_\gamma,\epsilon)\end{aligned} \tag{A4}$$

in the s channel and

$$\begin{aligned}\hat{A}_u^{\frac{1}{2}^+} &= FD(p)m\Omega(p_\gamma,\epsilon),\\ \hat{B}_u^{\frac{1}{2}^+} &= FD(p)m\Sigma(p_\gamma,\epsilon),\\ \hat{C}_u^{\frac{1}{2}^+} &= FD(p)\Omega_3(p_\gamma,\epsilon,p),\\ \hat{D}_u^{\frac{1}{2}^+} &= FD(p)\Sigma_3(p_\gamma,\epsilon,p)\end{aligned} \tag{A5}$$

in the u channel, where p_γ and ϵ are the photon four-momentum and polarization, m and p are the mass and four-momentum of the intermediate baryon, and D is the propagator denominator defined by

$$D(p) = (p^2 - m^2 + im\Gamma)^{-1}. \tag{A6}$$

The coupling products F are defined by Eqs. (53). Note that the intermediate baryon width Γ in Eq. (A6) is zero in the Born terms. For an intermediate proton, there are additional contributions to the operators from the charge coupling. These are given by

$$\begin{aligned}\hat{A}^{\text{charge}} &= eg_{\Lambda Kp}D(p)\Omega(p,\epsilon),\\ \hat{B}^{\text{charge}} &= eg_{\Lambda Kp}D(p)\Sigma(p,\epsilon),\\ \hat{C}^{\text{charge}} &= eg_{\Lambda Kp}D(p)m\sigma\cdot\epsilon,\\ \hat{D}^{\text{charge}} &= 0.\end{aligned} \tag{A7}$$

For contributions with intermediate spin $\frac{3}{2}$ resonances, we define the coupling parameters

$$\begin{aligned}\beta_1 &= F_1 + F_2,\\ \beta_2 &= F_2 - 2F_1,\\ \beta_3 &= 3F_1 - F_2\end{aligned} \tag{A8}$$

with

$$\begin{aligned}F_1 &= \frac{G^1}{2m_B m_\pi}D(p),\\ F_2 &= \frac{mG^2}{(2m_B)^2 m_\pi}D(p),\end{aligned} \tag{A9}$$

where m_B is the mass of the ground-state baryon at the photon vertex and G^1 and G^2 are the couplings defined by Eqs. (54). With these definitions, the operators for intermediate resonances of positive parity and spin $\frac{3}{2}$ are given by

$$\begin{aligned}\hat{A}_s^{\frac{3}{2}^+} &= \frac{1}{3}[\beta_1\Omega(p_K,k_1) + 2F_1(p_K\cdot p)\Omega(p_\gamma,\epsilon)\\ &\quad - 3\Omega(p,q_1) - 2F_1\Omega_4(p,p_K,p_\gamma,\epsilon)],\\ \hat{B}_s^{\frac{3}{2}^+} &= \frac{1}{3}[\beta_1\Sigma(p_K,k_1) + 2F_1(p_K\cdot p)\Sigma(p_\gamma,\epsilon) - 3\Sigma(p,q_1)\\ &\quad - 2F_1\Sigma_4(p,p_K,p_\gamma,\epsilon) - 3F_2(p_K\cdot k_1)],\\ \hat{C}_s^{\frac{3}{2}^+} &= \frac{1}{3m}[\beta_1\Omega_3(p,p_K,k_1) + 2F_1(p_K\cdot p)\Omega_3(p,p_\gamma,\epsilon)\\ &\quad + 3F_2(p_K\cdot k_1)\sigma\cdot\mathbf{p} + 3m^2\sigma\cdot\mathbf{q}_1\\ &\quad - 2m^2F_1\Omega_3(p_K,p_\gamma,\epsilon)],\\ \hat{D}_s^{\frac{3}{2}^+} &= \frac{1}{3m}[\beta_1\Sigma_3(p,p_K,k_1) + 2F_1(p_K\cdot p)\Sigma_3(p,p_\gamma,\epsilon)\\ &\quad - 3F_2(p_K\cdot k_1)E - 3m^2q_1^0\\ &\quad - 2m^2F_1\Sigma_3(p_K,p_\gamma,\epsilon)]\end{aligned} \tag{A10}$$

in the s channel and

$$\begin{aligned}\hat{A}_u^{\frac{3}{2}^+} &= \frac{1}{3}[-\beta_3\Omega(k_1,p_K) - 2F_1(p_K\cdot p)\Omega(\epsilon,p_\gamma)\\ &\quad + 3\Omega(p,q_1) + 2F_1\Omega_4(p,\epsilon,p_\gamma,p_K)],\\ \hat{B}_u^{\frac{3}{2}^+} &= \frac{1}{3}[-\beta_3\Sigma(k_1,p_K) - 2F_1(p_K\cdot p)\\ &\quad \Sigma(\epsilon,p_\gamma) + 3\Sigma(p,q_1)\\ &\quad + 2F_1\Sigma_4(p,\epsilon,p_\gamma,p_K) - 3\beta_2(p_K\cdot k_1)],\\ \hat{C}_u^{\frac{3}{2}^+} &= \frac{1}{3m}[-\beta_1\Omega_3(p,k_1,p_K) - 2F_1(p_K\cdot p)\Omega_3(p,\epsilon,p_\gamma)\\ &\quad - 3F_2(p_K\cdot k_1)\sigma\cdot\mathbf{p} - 3m^2\sigma\cdot\mathbf{q}_2\\ &\quad + 2m^2F_1\Omega_3(\epsilon,p_\gamma,p_K)],\\ \hat{D}_u^{\frac{3}{2}^+} &= \frac{1}{3m}\big[-\beta_1\Sigma_3(p,k_1,p_K) - 2F_1(p_K\cdot p)\Sigma_3(p,\epsilon,p_\gamma)\\ &\quad + 3F_2(p_K\cdot k_1)E + 3m^2q_2^0\\ &\quad + 2m^2F_1\Sigma_3(\epsilon,p_\gamma,p_K)\big]\end{aligned} \tag{A11}$$

in the u channel, where E is the energy of the intermediate resonance, p_K is the kaon four-momentum,

$$\begin{aligned}k_1 &= (p\cdot\epsilon)p_\gamma - (p\cdot p_\gamma)\epsilon,\\ k_2 &= (p_K\cdot\epsilon)p_\gamma - (p_K\cdot p_\gamma)\epsilon,\end{aligned} \tag{A12}$$

and

$$\begin{aligned}q_1 &= F_1k_2 + \beta_2\frac{p_K\cdot p}{3m^2}k_1,\\ q_2 &= F_1k_2 - F_2\frac{p_K\cdot p}{3m^2}k_1.\end{aligned} \tag{A13}$$

For contributions with intermediate spin $\frac{5}{2}$ resonances, we define the coupling parameters

$$\begin{aligned}F_1 &= \frac{G^1}{2m_B(m_\pi)^3}D(p),\\ F_2 &= \frac{mG^2}{(2m_B)^2(m_\pi)^3}D(p),\end{aligned} \tag{A14}$$

where G^1 and G^2 are the coupling products given by Eqs. (54) and the linear combinations

$$\begin{aligned}\xi_1 &= b_1p_\gamma - b_2\epsilon,\\ \xi_2 &= a_1p_\gamma - a_2\epsilon,\\ \zeta &= q\cdot\epsilon p_\gamma + q\cdot p_\gamma\epsilon,\end{aligned} \tag{A15}$$

where

$$\begin{aligned} a_1 &= 2q\cdot p_\gamma p_B\cdot\epsilon - q\cdot\epsilon p_B\cdot p_\gamma,\\ a_2 &= q\cdot p_\gamma p_B\cdot p_\gamma,\\ b_1 &= q\cdot p_\gamma p\cdot\epsilon + q\cdot\epsilon p\cdot p_\gamma,\\ b_2 &= 2q\cdot p_\gamma p\cdot p_\gamma \end{aligned} \tag{A16}$$

with

$$q = p_K - \beta p \tag{A17}$$

and

$$\beta = \frac{p\cdot p_K}{m^2}. \tag{A18}$$

Four other useful combinations are

$$\begin{aligned} c_1 &= q\cdot\epsilon p_K\cdot p_\gamma + q\cdot p_\gamma p_K\cdot\epsilon - p_K\cdot p_\gamma p_K\cdot\epsilon\\ &\quad + \frac{1}{5}\beta_K p\cdot\epsilon p\cdot p_\gamma,\\ c_2 &= (2q\cdot p_\gamma - p_K\cdot p_\gamma)p_K\cdot\ p_\gamma + \frac{1}{5}\beta_K(p\cdot p_\gamma)^2,\\ c_3 &= \frac{a_1 p\cdot p_\gamma - a_2 p\cdot\epsilon}{m^2},\\ c_4 &= a_1 p_K\cdot p_\gamma - a_2 p_K\cdot\epsilon + p_K\cdot\ p_\gamma(p_B\cdot p_\gamma p_K\\ &\quad\cdot\epsilon - p_B\cdot\epsilon p_K\cdot p_\gamma) + \frac{1}{5}\beta_K p\cdot p_\gamma\\ &\quad (p\cdot p_\gamma p_B\cdot\epsilon - p\cdot\epsilon p_B\cdot p_\gamma) \end{aligned} \tag{A19}$$

with

$$\beta_K = \frac{m_K^2 + 4(\beta m)^2}{m^2}. \tag{A20}$$

In terms of these quantities, we have for positive-parity spin $\frac{5}{2}$ resonances

$$\begin{aligned} \hat{A}_s^{\frac{5}{2}^+} &= F_1[c_1\Omega(p,\ p_\gamma) - c_2\Omega(p,\epsilon)] + \frac{1}{5}F_2[c_3\Omega(q,\ p)\\ &\quad - \Omega(q,\xi_2)] + \frac{1}{5}F_1\Bigg[\frac{1}{m^2}\Omega_4(p,q,\ p,\xi_1) + 2q\\ &\quad\cdot p_\gamma\Omega_4(p,q,\ p_\gamma,\epsilon) - \Omega_4(p,q,\zeta,\ p_\gamma)\Bigg],\\ \hat{B}_s^{\frac{5}{2}^+} &= F_2c_4 + F_1[c_1\Sigma(p,\ p_\gamma) - c_2\Sigma(p,\epsilon)]\\ &\quad + \frac{1}{5}F_2[c_3\Sigma(q,\ p) - \Sigma(q,\xi_2)]\\ &\quad + \frac{1}{5}F_1\Bigg[\frac{1}{m^2}\Sigma_4(p,q,\ p,\xi_1)\\ &\quad + 2q\cdot p_\gamma\Sigma_4(p,q,\ p_\gamma,\epsilon) - \Sigma_4(p,q,\zeta,\ p_\gamma)\Bigg],\\ \hat{C}_s^{\frac{5}{2}^+} &= F_2\frac{c_4}{m}\sigma\cdot p + F_1m[c_1\sigma\cdot p_\gamma - c_2\sigma\cdot\epsilon]\\ &\quad - \frac{1}{5m}F_2[c_3\Omega_3(p,q,\ p) - \Omega_3(p,q,\xi_2)]\\ &\quad - \frac{1}{5}F_1\Bigg[\frac{1}{m}\Omega_3(q,\ p,\xi_1)\\ &\quad + 2q\cdot p_\gamma m\Omega_3(q,\ p_\gamma,\epsilon) - m\Omega_3(q,\zeta,\ p_\gamma)\Bigg],\\ \hat{D}_s^{\frac{5}{2}^+} &= -F_2c_4\frac{E}{m} - F_1c_1mE_\gamma\\ &\quad - \frac{1}{5m}F_2[c_3\Sigma_3(p,q,\ p) - \Sigma_3(p,q,\xi_2)]\\ &\quad - \frac{1}{5}F_1\Bigg[\frac{1}{m}\Sigma_3(q,\ p,\xi_1) + 2q\\ &\quad\cdot p_\gamma m\Sigma_3(q,\ p_\gamma,\epsilon) - m\Sigma_3(q,\zeta,\ p_\gamma)\Bigg] \end{aligned} \tag{A21}$$

in the s channel and

$$\begin{aligned} \hat{A}_u^{\frac{5}{2}^+} &= F_1[c_1\Omega(p_\gamma,\ p) - c_2\Omega(\epsilon,\ p)] + \frac{1}{5}F_2[c_3\Omega(p,q)\\ &\quad - \Omega(\xi_2,q)] + \frac{1}{5}F_1\Bigg[\frac{1}{m^2}\Omega_4(\xi_1,\ p,\ p,\ q)\\ &\quad + 2q\cdot p_\gamma\Omega_4(\epsilon,\ p,\ p_\gamma,q) - \Omega_4(p_\gamma,\ p,\zeta,q)\Bigg],\\ \hat{B}_u^{\frac{5}{2}^+} &= F_2c_4 + F_1[c_1\Sigma(p_\gamma,\ p) - c_2\Sigma(\epsilon,\ p)] + \frac{1}{5}F_2[c_3\Sigma(p,q)\\ &\quad - \Sigma(\xi_2,q)] + \frac{1}{5}F_1\Bigg[\frac{1}{m^2}\Sigma_4(\xi_1,\ p,\ p,\ q)\\ &\quad + 2q\cdot p_\gamma\Sigma_4(\epsilon,\ p,\ p_\gamma,q) - \Sigma_4(p_\gamma,\ p,\zeta,q)\Bigg],\\ \hat{C}_u^{\frac{5}{2}^+} &= -F_2\frac{c_4}{m}\sigma\cdot p + F_1m[c_2\sigma\cdot\epsilon - c_1\sigma\cdot p_\gamma]\\ &\quad + \frac{1}{5m}F_2[c_3\Omega_3(p,\ p,q) - \Omega_3(p,\xi_2,q)]\\ &\quad + \frac{1}{5}F_1\Bigg[\frac{1}{m}\Omega_3(\xi_1,\ p,q)\\ &\quad + 2q\cdot p_\gamma m\Omega_3(\epsilon,\ p_\gamma,q) - m\Omega_3(p_\gamma,\zeta,q)\Bigg],\\ \hat{D}_u^{\frac{5}{2}^+} &= F_2c_4\frac{E}{m} + F_1c_1mE_\gamma + \frac{1}{5m}F_2[c_3\Sigma_3(p,\ p,q)\\ &\quad - \Sigma_3(p,\xi_2,q)] + \frac{1}{5}F_1\Bigg[\frac{1}{m}\Sigma_3(\xi_1,\ p,q)\\ &\quad + 2q\cdot p_\gamma m\Sigma_3(\epsilon,\ p_\gamma,q) - m\Sigma_3(p_\gamma,\zeta,q)\Bigg] \end{aligned} \tag{A22}$$

in the u channel.

For intermediate baryons of negative parity, the $\hat{A}$ and $\hat{B}$ operators are given by the same expressions as for intermediate baryons of positive parity and the same spin, whereas the $\hat{C}$ and $\hat{D}$ operators are given by expressions that are the negatives of the corresponding positive-parity expressions.

For the t channel, we define the coupling parameters

$$\begin{aligned} \alpha^V &= \frac{G^V_{K^\star}}{m_{\rm sc}}D(p),\\ \alpha^T &= \frac{G^T_{K^\star}}{m_{\rm sc}(m_p + m_\Lambda)}D(p), \end{aligned} \tag{A23}$$

where $m_{\rm sc}$ is the same scaling mass that appears in Eqs. (6) and (8) and the $G_{K^\star}$ are the coupling products defined by

Eqs. (56). In terms of these parameters, the t-channel operators are given by

$$\begin{aligned}\hat{A}^t_K &= 0,\\ \hat{B}^t_K &= e g_{\Lambda K p} D(p),\\ \hat{C}^t_K &= 0,\\ \hat{D}^t_K &= 0\end{aligned} \tag{A24}$$

for an intermediate kaon,

$$\begin{aligned}\hat{A}^t_{K^\star} &= i\alpha^T(Ef - \sigma\cdot\mathbf{p}\sigma\cdot\xi),\\ \hat{B}^t_{K^\star} &= -i\alpha^T(E\sigma\cdot\xi - f\sigma\cdot\mathbf{p}),\\ \hat{C}^t_{K^\star} &= i\alpha^V f,\\ \hat{D}^t_{K^\star} &= -i\alpha^V\sigma\cdot\xi\end{aligned} \tag{A25}$$

for an intermediate $K^\star(892)$ resonance, and

$$\begin{aligned}\hat{A}^t_{K1} &= \alpha^T[\epsilon\cdot p_K\Omega(p,p_\gamma) + Ep_\gamma\cdot p_K\sigma\cdot\epsilon],\\ \hat{B}^t_{K1} &= \alpha^T[\epsilon\cdot p_K\Sigma(p,p_\gamma) + p_\gamma\cdot p_K\sigma\cdot\mathbf{p}\sigma\cdot\epsilon],\\ \hat{C}^t_{K1} &= \alpha^V[p_\gamma\cdot p_K\sigma\cdot\epsilon - \epsilon\cdot p_K\sigma\cdot\mathbf{p}_\gamma],\\ \hat{D}^t_{K1} &= \alpha^V\epsilon\cdot p_K E_\gamma\end{aligned} \tag{A26}$$

for an intermediate $K1(1270)$ resonance, where p and E are the four-momentum and energy of the intermediate meson,

$$f = \epsilon\cdot\mathbf{p}_\gamma\times\mathbf{p}_K, \tag{A27}$$

and

$$\xi = \epsilon\times(E_K\mathbf{p}_\gamma - E_\gamma\mathbf{p}_K). \tag{A28}$$

[1] H. Thom, Phys. Rev. **151**, 1322 (1966).
[2] F. M. Renard and Y. Renard, Nucl. Phys. **B1**, 389 (1967); Phys. Lett. **B24**, 159 (1967); Nucl. Phys. **B25**, 490 (1971); Y. Renard, *ibid.* **B40**, 499 (1972).
[3] H. Thom, E. Gabathuler, D. Jones, B. D. McDaniel, and W. M. Woodward, Phys. Rev. Lett. **11**, 433 (1963); M. Grilli, L. Mezzetti, M. Nigro, and E. Schiavuta, Nuovo Cim. **38**, 1467 (1965); D. E. Groom and J. H. Marshall, Phys. Rev. **159**, 1213 (1967); T. Fujii *et al.*, Phys. Rev. D **2**, 439 (1970).
[4] M. Q. Tran *et al.*, Phys. Lett. **B445**, 20 (1998); S. Goers *et al.*, *ibid.* **B464**, 331 (1999); K. H. Glander *et al.*, Eur. Phys. J. A **19**, 251 (2004).
[5] R. G. T. Zegers *et al.*, Phys. Rev. Lett. **91**, 092001 (2003); M. Sumihama *et al.*, Phys. Rev. C **73**, 035214 (2006).
[6] G. Niculescu *et al.*, Phys. Rev. Lett. **81**, 1805 (1998); L. Teodorescu *et al.*, Nucl. Phys. **A658**, 362 (1999); R. M. Mohring *et al.*, Phys. Rev. C **67**, 055205 (2003).
[7] D. S. Carman *et al.*, Phys. Rev. Lett. **90**, 131804 (2003); D. S. Carman *et al.*, Phys. Rev. C **79**, 065205 (2009).
[8] J. W. C. McNabb *et al.*, Phys. Rev. C **69**, 042201(R) (2004).
[9] A. Lleres *et al.*, Eur. Phys. J. A **31**, 79 (2007); A. D'Angelo *et al.*, *ibid.* **31**, 441 (2007).
[10] R. Bradford *et al.*, Phys. Rev. C **73**, 035202 (2006).
[11] R. Bradford *et al.*, Phys. Rev. C **75**, 035205 (2007).
[12] P. Ambrozewicz *et al.*, Phys. Rev. C **75**, 045203 (2007).
[13] R. Nasseripour *et al.*, Phys. Rev. C **77**, 065208 (2008).
[14] R. A. Adelseck, C. Bennhold, and L. E. Wright, Phys. Rev. C **32**, 1681 (1985).
[15] R. A. Adelseck and L. E. Wright, Phys. Rev. C **38**, 1965 (1988); R. A. Adelseck and B. Saghai, *ibid.* **42**, 108 (1990).
[16] R. A. Williams, C.-R. Ji, and S. R. Cotanch, Phys. Rev. C **46**, 1617 (1992).
[17] T. Mart, C. Bennhold, and C. E. Hyde-Wright, Phys. Rev. C **51**, R1074 (1995); H. Haberzettl, C. Bennhold, T. Mart, and T. Feuster, *ibid.* **58**, R40 (1998); T. Mart and C. Bennhold, Nucl. Phys. **A639**, 237c (1998); H. Haberzettl, C. Bennhold, and T. Mart, Acta Phys. Pol. B **31**, 2387 (2000); Nucl. Phys. **A684**, 475c (2001).
[18] T. Mart and C. Bennhold, Phys. Rev. C **61**, 012201(R) (1999).
[19] M. K. Cheoun, B. S. Han, B. G. Yu, and Il-Tong Cheon, Phys. Rev. C **54**, 1811 (1996); Bong Son Han, Myung Ki Cheoun, K. S. Kim, and Il-Tong Cheon, Nucl. Phys. **A691**, 713 (2001).
[20] J. C. David, C. Fayard, G. H. Lamot, and B. Saghai, Phys. Rev. C **53**, 2613 (1996).
[21] T. Mizutani, C. Fayard, G.-H. Lamot, and B. Saghai, Phys. Rev. C **58**, 75 (1998).
[22] S. S. Hsiao, D. H. Lu, and Shin Nan Yang, Phys. Rev. C **61**, 068201 (2000).
[23] Wen Tai Chiang, F. Tabakin, T-S. H. Lee, and B. Saghai, Phys. Lett. **B517**, 101 (2001).
[24] S. Janssen, J. Ryckebusch, W. Van Nespen, D. Debruyne, and T. Van Cauteren, Eur. Phys. J. A **11**, 105 (2001); S. Janssen, J. Ryckebusch, D. Debruyne, and T. Van Cauteren, Phys. Rev. C **65**, 015201 (2001); **66**, 035202 (2002); S. Janssen, J. Ryckebusch, and T. Van Cauteren, *ibid.* **67**, 052201(R) (2003); S. Janssen, D. G. Ireland, and J. Ryckebusch, Phys. Lett. **B562**, 51 (2003).
[25] O. V. Maxwell, Phys. Rev. C **69**, 034605 (2004).
[26] O. V. Maxwell, Phys. Rev. C **70**, 044612 (2004).
[27] O. V. Maxwell, Phys. Rev. C **76**, 014621 (2007).
[28] A. Usov and O. Scholten, Phys. Rev. C **72**, 025205 (2005).
[29] A. V. Sarantsev, V. A. Nikonov, A. V. Anisovich, E. Klempt, and U. Thoma, Eur. Phys. J. A **25**, 441 (2005); A. V. Anisovich, V. Kleber, E. Klempt, V. A. Nikonov, A. V. Sarantsev, and U. Thoma, *ibid.* **34**, 243 (2007); V. A. Nikonov, A. V. Anisovich, E. Klempt, A. V. Sarantsev, and U. Thoma, Phys. Lett. **B662**, 245 (2008).
[30] N. Kaiser, T. Waas, and W. Weise, Nucl. Phys. **A612**, 297 (1997).
[31] T. Feuster and U. Mosel, Phys. Rev. C **59**, 460 (1999).
[32] B. Julia-Diaz, B. Saghai, T. S. H. Lee, and F. Tabakin, Phys. Rev. C **73**, 055204 (2006).
[33] See, for example, the discussion in T. Mart and A. Sulaksono, Phys. Rev. C **74**, 055203 (2006); P. Bydžovsky and T. Mart, *ibid.* **76**, 065202 (2007).
[34] M. Benmerrouche, R. M. Davidson, and Nimai C. Mukhopadhyay, Phys. Rev. C **39**, 2339 (1989).
[35] W. M. Yao *et al.*, J. Phys. G **33**, 1 (2006).
[36] S. Capstick and W. Roberts, Phys. Rev. D **58**, 074011 (1998).
[37] J. J. deSwart, Rev. Mod. Phys. **35**, 916 (1963).
[38] O. Dumbrajs, R. Koch, H. Pilkuhn, G. C. Oades, H. Behrens, J. J. de Swart, and P. Kroll, Nucl. Phys. **B216**, 277 (1983).
[39] I. J. General and S. R. Cotanch, Phys. Rev. C **69**, 035202 (2004).
[40] F. J. Klein *et al.*, Jefferson Lab Experiment E02-112.
[41] A. Lleres *et al.*, Eur. Phys. J. A **39**, 149 (2009).